Global Synchronous Pulse Width Modulation of Distributed Inverters

Tao Xu and Feng Gao, *Member, IEEE*

***Abstract*—Traditionally, the parallel-connected multileg inverter could assume the interleaved pulse width modulation (PWM) to attenuate the high-frequency harmonics by using a single controller to generate the corresponding interleaved switching sequences. However, the interleaved PWM cannot be employed in multiple distributed independent inverters installed at different locations with their own controllers because the multiple independent controllers cannot work synchronously and the operational conditions are different among the distributed inverters. The summed current harmonics of multiple distributed inverters could vary at the point of common coupling (PCC) and worsen the power quality of consumers. This paper, therefore, proposes a global synchronous PWM method for the distributed inverters to attenuate the high-frequency current harmonics at PCC. The optimal interleaved switching angles among the distributed inverters are calculated by fully considering line impedances, modulation indexes, switching frequencies, the number of distributed inverters, etc. Particle swarm optimization method is assumed to find the optimal solution. Then, the low-frequency synchronization operation will synchronize the multiple PWM switching sequences in the wanted variation range. Experimental results are presented to prove the validity of this method.**

***Index Terms*—Current harmonics, distributed inverters, global modulation, synchronous pulse width modulation.**

NOMENCLATURE

$C_{\rm peak}$	Peak value of carrier counter.
cyc	Cycle index of PSO.
$cyc_{\max}$	Maximum cycle index.
cyc_h	Historical cycle index.
$f_{{\rm DSP}M}$	Working frequency of DSP in controller *M*.
$f_{{\rm PWM}M}$	PWM frequency of inverter *M*.
f_c	Switching frequency.
f_1	Fundamental frequency.
$f_{\rm syn}$	Frequency of synchronous signals.
$f_{\rm synmin}$	Minimum $f_{\rm syn}$.
f	Frequency of specific harmonic current.
$f_{\rm cM}$	Switching frequency of ${\rm PWM}_M$.
f_{1M}	Fundamental frequency of ${\rm PWM}_M$.
i_M	Output current of inverter *M*.
i_{1M}	Fundamental component of $i_{\rm M}$.
$i_{\rm hM}$	Total harmonic currents of $i_{\rm M}$.
$i_{\rm hMf}$	Specific harmonic current of $i_{\rm M}$ with harmonic frequency *f*.
$\dot{I}_{\rm hMf}$	Phasor of $i_{\rm hMf}$.
$i_{\rm sum}$	Total current flowing from PCC to grid.
$i_{\rm 1sum}$	Fundamental component of $i_{\rm sum}$.
$i_{h\rm sum}$	Sum of harmonic currents of $i_{\rm sum}$.
$i_{h{\rm sum}f}$	Specific harmonic current of $i_{\rm sum}$ with harmonic frequency *f*.
$\dot{I}_{h{\rm sum}f}$	Phasor of $i_{h{\rm sum}f}$.
$I_{\rm M}, I_{1M}, I_{\rm hM}, I_{\rm hMf}$	RMS values of $i_{\rm M}, i_{1M}, i_{\rm hM}, i_{\rm hMf}$.
$I_{\rm sum}, I_{\rm 1sum}, I_{h\rm sum}, I_{h{\rm sum}f}$	RMS values of $i_{\rm sum}, i_{\rm 1sum}, i_{h\rm sum}, i_{h{\rm sum}f}$.
$k_{\rm M}$	Carrier frequency multiple of inverter *M*.
$L_{\rm M}$	Sum of filter inductance and feeder inductance.
M	Numerical order of inverter or its controller ($M = 1, \ldots, N$).
$m_{\rm M}$	Modulation index of inverter *M*.
$n_{\rm M}$	Fundamental frequency multiple of inverter *M*.
N	Quantity of distributed inverters.
${\rm PWM}_{\rm M}$	PWM sequence of inverter *M*.
$P_{\rm M}$	Active power of inverter *M*.
$Q_{\rm M}$	Reactive power of inverter *M*.
${\rm THD}_{\rm M}$	THD of $i_{\rm M}$.
${\rm THD}_{\rm sum}$	THD of $i_{\rm sum}$.
$t_{\rm change}$	Time to reach the optimal phase shift angle.
$t_{\rm changemax}$	Maximum $t_{\rm change}$.
$u_{\rm hM}$	Output harmonic voltage of inverter *M*.
$u_{\rm hMf}$	Specific harmonic voltage of $u_{\rm hM}$ with harmonic frequency *f*.
$\dot{U}_{\rm hMf}$	Phasor of $u_{\rm hMf}$.
$U_{{\rm dc}M}$	DC bus voltage of inverter *M*.
$\vec{v}_x\ (cyc)$	Velocity vector of particle *x* at cycle index *cyc*.
$v_{\max}$	The maximum velocity of particles.
x	Numerical order of particle.

Manuscript received August 4, 2015; accepted November 18, 2015. Date of publication November 30, 2015; date of current version March 25, 2016. This paper was presented in part at the *ECCE Asia* (*ICPE 2015-ECCE Asia*) 2015, Seoul, Korea, June 1–5, 2015. Recommended for publication by Associate Editor B. Wang.

The authors are with the Key Lab of Power System Intelligent Dispatch and Control, Ministry of Education, Shandong University, Jinan 250061, China (e-mail: xutaojason@163.com; fgao@sdu.edu.cn).

Color versions of one or more of the figures in this paper are available online at http://ieeexplore.ieee.org.

Digital Object Identifier 10.1109/TPEL.2015.2504361

$X_{\max}$	Quantity of particles.
θ_{hMf}	Phase angle between $\dot{U}_{\mathrm{hMf}}$ and $\dot{I}_{\mathrm{hMf}}$.
φ_{hMf}	Phase angle of $\dot{I}_{\mathrm{hMf}}$.
$\varphi_{h\mathrm{sum}f}$	Phase angle of $\dot{I}_{h\mathrm{sum}f}$.
$\varphi_{\mathrm{PWM}M}$	Phase-shift angle between $\mathrm{PWM_M}$ and $\mathrm{PWM_1}$.
$\varphi_{\mathrm{PWM}M\,\mathrm{best}}$	Optimal phase-shift angle.
$\Delta\varphi_{\max}$	Maximum allowable range of phase deviation.
$\Delta\varphi_{1s}$	Maximum phase deviation between two PWM signals per second.
φ_{1M}	Phase-shift angle between fundamental voltage of inverter M and fundamental voltage of inverter 1.
$\vec{\varphi}_x\ (cyc)$	Phase position vector of particle x at cycle index cyc.
$\vec{\varphi}_{g\mathrm{best}}$	Historical best position of all particles.
$\vec{\varphi}_{x\mathrm{best}}$	Historical best position of particle x.

I. Introduction

NOWADAYS, a large number of distributed generation (DG) units have being integrated into the distribution power grid driven by the environmental issues, economical factors, and social interests [1]–[3]. Most of the distributed generators are connected to the grid through the grid-tied inverters as shown in Fig. 1. The injected currents from DGs unavoidably contain the high-frequency harmonics. An *LC* or *LCL* filter could be employed to attenuate the current harmonics of single inverter [4]–[11]. Alternatively, a multileg inverter with the interleaved pulse width modulation (PWM) can achieve the similar performance either [12]–[15]. The interleaving technology leads to the reduction of filter size and cost. But the traditional multileg circuits are supplied by a common dc source and controlled by one controller. Perreault and Kassakian [16] employed the distributed approach to interleave the power converter cells with their own controllers. But they were also supplied by a common dc source. Beechner and Sun [17] and Schuck and Pilawa-Podgurski [18] explored the phase-shifting method for nonuniform duty ratios and different input sources for each phase. But this method can only be used in dc–dc converter. Therefore, for the scenario, where multiple distributed inverters connect to the same point of common coupling (PCC), the current interleaving techniques cannot be directly employed and the current harmonics would be randomly summed and induce the current and voltage distortions. The individual inverter cannot guarantee its output current to be purely sinusoidal under the tradeoff among switching frequency, cost, and efficiency. Besides, the active power filter can only compensate the low-order harmonics limited by its control bandwidth, leaving the high-frequency harmonics unchanged [19], [20]. Therefore, the state-of-the-art techniques cannot solve the problem of high-frequency current harmonics accumulation in the distribution grid with the high-density distributed inverters.

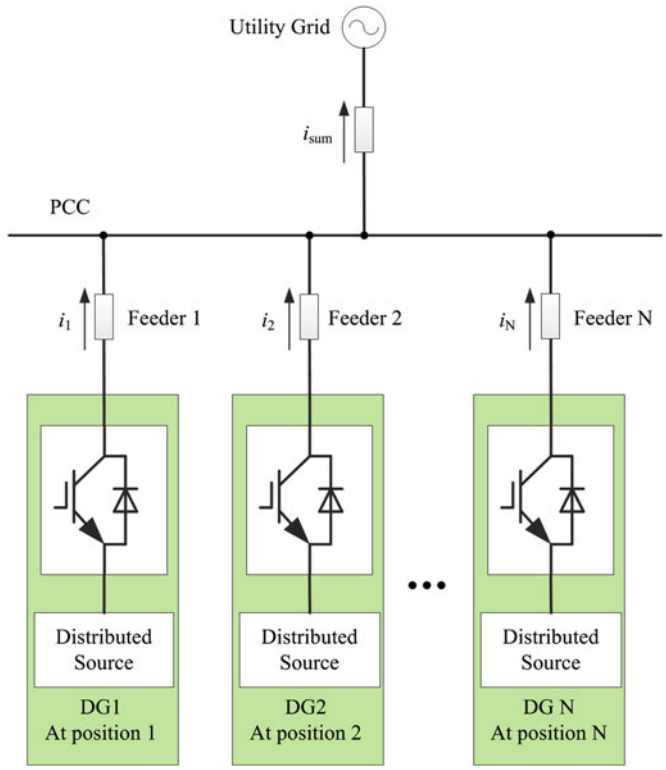

Fig. 1. Illustration of distributed inverters connected to a PCC.

This paper proposes a global synchronous PWM (GSPWM) method to attenuate the high-frequency current harmonics at PCC realized by a simple communication and an adaptive control method with the known operating parameters, including switching frequency, output impedance, grid voltage, modulation mode, active power, reactive power, and dc-link voltage per inverter. The GSPWM does not deteriorate the output performance per distributed inverter once the communication fails since the proposed method does not change the switching frequency and control algorithm of individual inverter and the communication system only upload the operating parameters per inverter to the master unit and transfer the synchronous pulses and the interleaved carrier angles from master unit to slave inverters. The communication channel can be RS485, RS232, power line carrier (PLC), or optical fiber depending on the communication distance and accuracy. And the GSPWM is superior for below applications as examples:

1) large scale PV station with multiple same type inverters under the similar operation conditions;
2) power electronics ac microgrid with multiple inverters working under different conditions.

For a small area application, where the communication reliability can be guaranteed, the GSPWM could also help reduce the output filter or switching frequency per individual inverter. To fully elaborate the operational principle and the advantages of GSPWM, the following sections describe the basic operational procedure and the adaptive carrier phase-shift strategy, respectively, regardless of the specific applications. Finally, the constructed experimental prototype with four independent

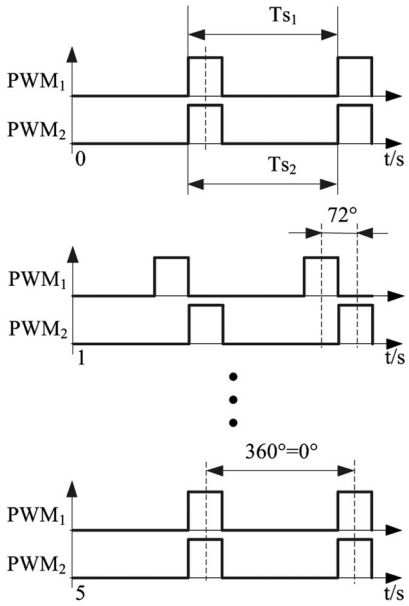

Fig. 2. Illustration of phase-shift phenomena between two PWM sequences.

TABLE I
PARAMETERS OF TWO SINGLE-PHASE INVERTERS

Inverter	Parameter	Value
1	Switching Frequency	$f_{c1} = 10.0001$ kHz
	Fundamental Frequency	$f_1 = 50$ Hz
	Modulation Mode	Unipolar
	DC Bus Voltage	$U_{dc1} = 200$ V
	Output Filter Inductances	$L_1 = 2$ mH
	THD of Output Current	$\mathrm{THD}_1 = 8.6\%$
2	Switching Frequency	$f_{c2} = 9.9999$ kHz
	Fundamental Frequency	$f_1 = 50$ Hz
	Modulation Mode	Unipolar
	DC Bus Voltage	$U_{dc2} = 200$ V
	Output Filter Inductances	$L_2 = 2$ mH
	THD of Output Current	$\mathrm{THD}_2 = 8.8\%$

single-phase inverters verifies the performance of the proposed GSPWM.

II. PRINCIPLE AND REALIZATION OF THE GSPWM

With the development of digital control technologies, most of the distributed inverters are controlled by the digital signal processers (DSPs) or other digital controllers. The crystal inside the digital controller is an important component, which resonates at a fixed frequency to synchronize the digital operation processes and the PWM generation function. But the crystal resonant frequency is significantly influenced by its working conditions. Hence, the PWM frequency is not exactly equal to what it has been set. Such phenomenon does not influence the operational performance of individual inverter. But when synchronizing the PWM sequences of multiple inverters, the unequal crystal frequencies among multiple digital controllers will unavoidably induce the PWM deviation. In specific, PPM is the deviation unit of crystal, where 1 PPM $= 10^{-6}$ [21]. In practice, the common deviation of crystal is 10 PPM. For a crystal with working frequency of 30 MHz, its real frequency ranges from 30 MHz–300 Hz to 30 MHz + 300 Hz. For example, assuming the TMSF28335 (DSP) as the digital controllers in two independent inverters, whose working frequency is 150 MHz, the real resonant frequencies inside these two DSPs can be

$$f_{\mathrm{DSP1}} = 150\ \mathrm{MHz} + 1.5\ \mathrm{kHz} \quad (1)$$

$$f_{\mathrm{DSP1}} = 150\ \mathrm{MHz} - 1.5\ \mathrm{kHz}. \quad (2)$$

When both PWM frequencies are 10 kHz, their real PWM frequencies could be

$$f_{\mathrm{PWM1}} = 10\ \mathrm{kHz} + 0.1\ \mathrm{Hz} \quad (3)$$

$$f_{\mathrm{PWM1}} = 10\ \mathrm{kHz} - 0.1\ \mathrm{Hz}. \quad (4)$$

The maximum difference between f_{PWM1} and f_{PWM2} is 0.2 Hz. Therefore the phase-shift angle between these two PWM sequences can change for 360° per 5 s. This phenomenon is shown in Fig. 2. Assuming the phase-shift angle between these two PWM signals is 0° at time 0 s. After 1 s, the phase-shift angle is 72°. After 5 s, the phase-shift angle becomes 360° = 0°. In implementation, when two inverters connect to the same PCC, the THD of current flowing from PCC to grid will change as time progresses. To present these phenomena clearly, this section uses Matlab/SIMULINK to simulate a system with two single-phase inverters connected to the same PCC and they are modulated using the unipolar modulation method with the switching frequencies of 10.0001 and 9.9999 kHz, respectively. The parameters of these two inverters are listed in Table I. The THD of current flowing from two inverters are 8.6% and 8.8%, respectively. The phase-shift angle between these two PWM signals is 0° at 0 s and will change for 360° every 5 s. The ripple of total current waveform changes as time progresses as illustrated in Fig. 3. Fig. 4 shows the trajectory of total current THD when the phase-shift angle changes from 0° to 360°, where the THD is minimum when the phase-shift angle between two PWM sequences is 90° or 270°. It is superior that the phase-shift angle could be 90° or 270° at any time. But unfortunately, the phase-shift angle continuously changes as time progresses in practice because their PWM frequencies are not exactly equal. Therefore, the PWM sequences in different inverters cannot have the fixed optimal phase-shift angle to minimize the THD of total current as the interleaved PWM implemented in a single multileg inverter.

To ensure the multiple PWM sequences among distributed inverters have the fixed optimal phase-shift angles to minimize the THD of total current, this paper proposes a GSPWM method, which includes the communication channels and a global synchronous unit (GSU) in implementation. Fig. 5 shows the configuration of distributed inverters with the communication channels and the GSU. The communication channels can be RS485, RS232, PLC or optical fiber. The choice of communication channel is determined by the working condition, cost, etc. The GSU could work in one digital controller among distributed inverters when the global synchronization function is not complex or in an independent processor when the global synchronization function is complicated. To clearly explain the working principle of this system, an example is presented below and illustrated in Fig. 6, where two single-phase inverters with unipolar

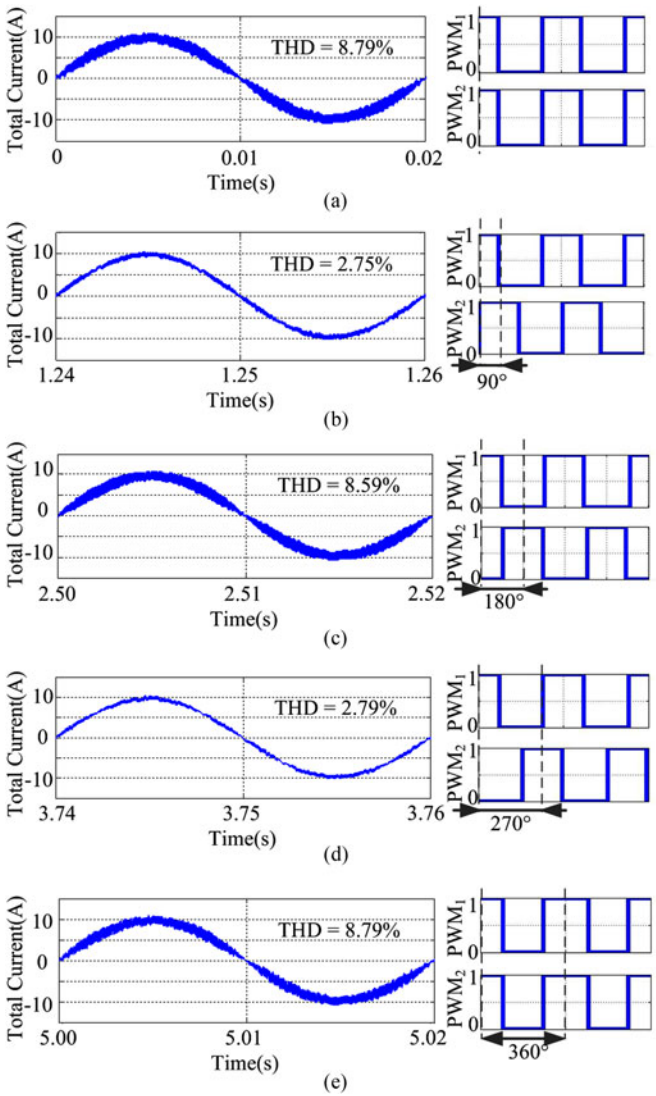

Fig. 3. Simulated waveforms of total current and PWM sequences of two distributed inverters under different phase-shift angles of (a) 0°, (b) 90°, (c) 180°, (d) 270°, and (e) 360°.

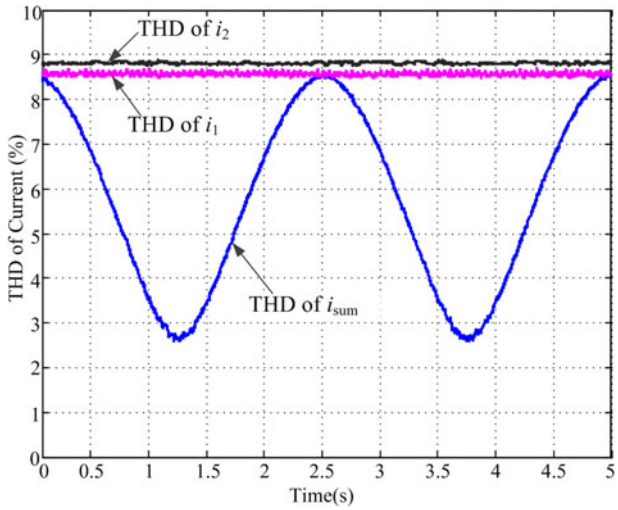

Fig. 4. THD trajectories of the total current $i_{\rm sum}$ and the output currents i_1 and i_2.

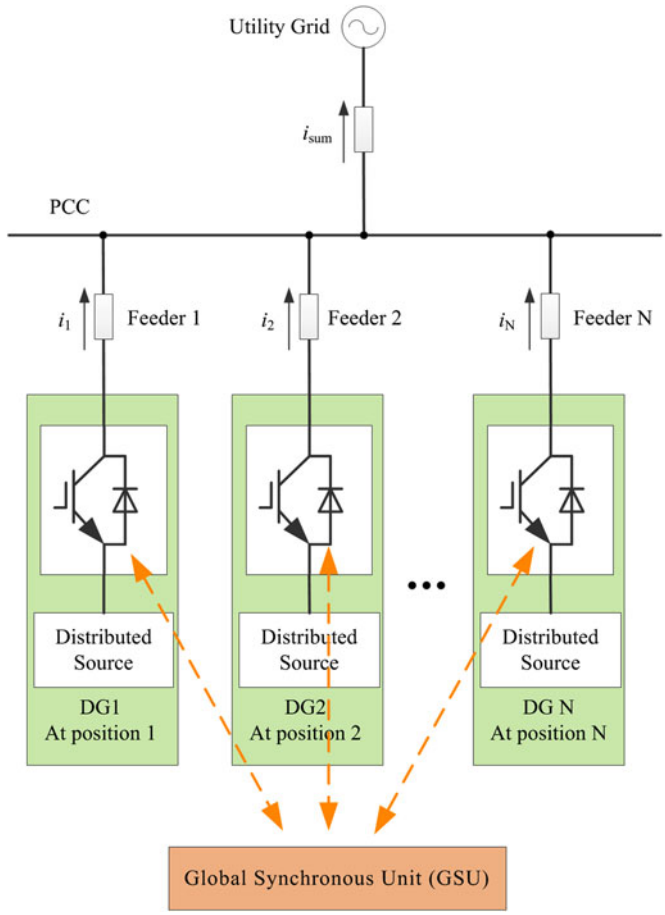

Fig. 5. Illustration of distributed inverters connected to a PCC with communication channel and GSU.

modulation mode connected to the same PCC work under the same operation condition and the GSU is realized in Controller 1. The working processes are classified into two main parts, which are *Calculation Part* and *Synchronization Part*, respectively.

A. Calculation Part

The calculation part contains three steps, which will be elaborated below one by one.

1) In general, Controller 2 will send its operational parameters (e.g., dc-link voltage, filter parameters, output power, the default switching frequency, etc.) to Controller 1 through the preset communication channel (e.g., RS485 in Fig. 6).
2) After Controller 1 receives the parameters sent from Controller 2, the GSU inside Controller 1 will start to calculate the optimal phase-shift angle between these two inverters and the sending frequency $f_{\rm syn}$ of synchronous signals. Since both inverters work under the same condition, the optimal phase-shift angle $\varphi_{\rm PWM2best}$ of PWM sequences in Controller 2 is easy to be derived as 90° or 270°, and 90° is chosen here. The phase-shift angle calculation method under a more complicated working condition will be presented in Section III. The specific

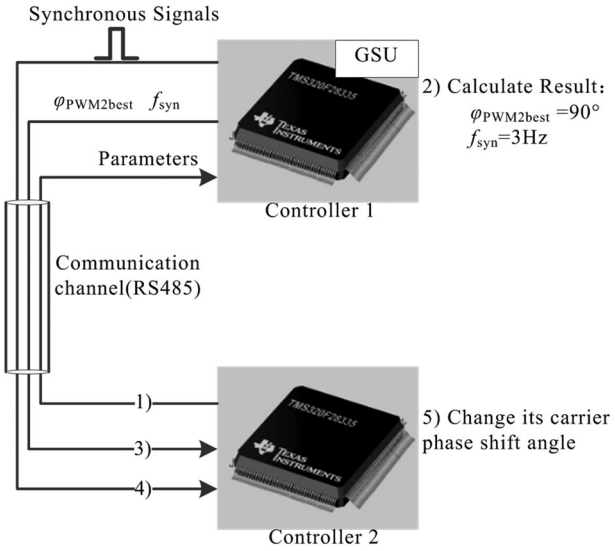

Fig. 6. General illustration of working principle with GSU and communication channel.

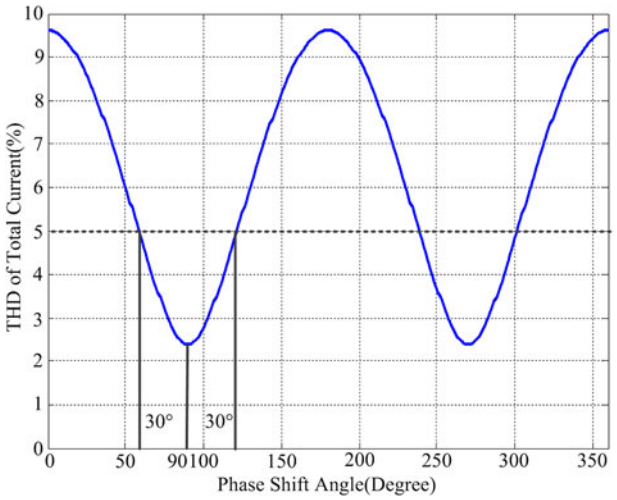

Fig. 7. Calculation result of total current THD when the phase-shift angle changes from 0° to 360°.

$f_{\rm syn}$ of synchronous signals depends on the deviation of both crystals, the switching frequencies, and communication speed. The higher $f_{\rm syn}$ will lead to better harmonic mitigation effect but need faster communication speed. On the other hand, the phase-shift angle will severely deviate from the optimal value if $f_{\rm syn}$ is low. The basic calculation principle of $f_{\rm syn}$ is introduced here. For a system with two inverters adopted above, Fig. 7 shows the calculated result of total current THD when phase-shift angle changes from 0° to 360°, which could be calculated by GSU according to the parameters of both inverters. For example, when the total current THD should be lower than 5%, the maximum allowable range of phase deviation $\Delta\varphi_{\rm max}$ is 30°. The phase angle deviation between these two PWM signals per second could be

$$\Delta\varphi_{1s} = \frac{2Err_{\rm cry}}{T_{\rm s}} \times 360^{\circ}. \tag{5}$$

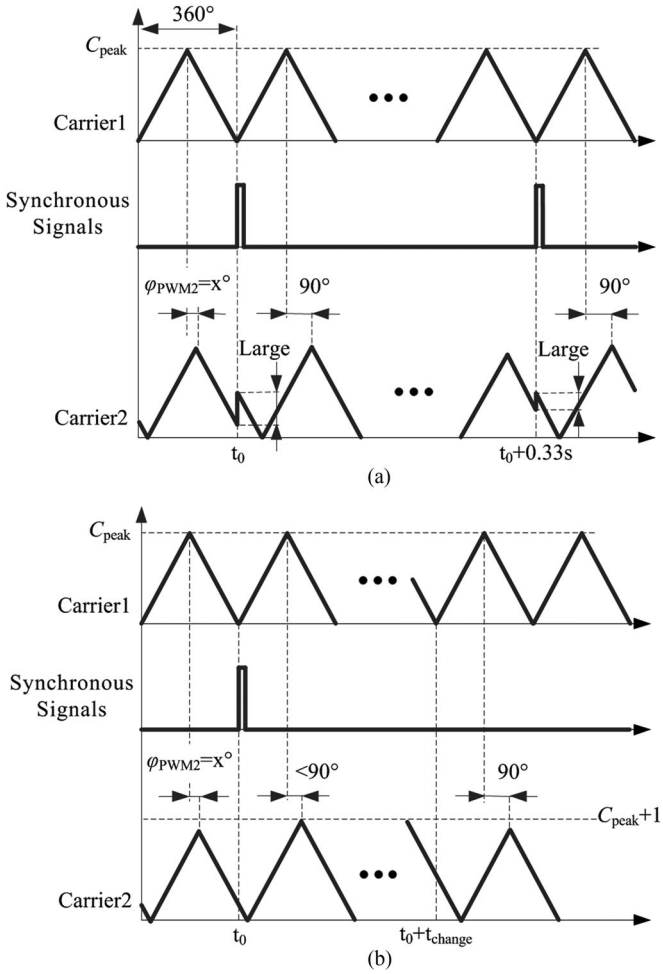

Fig. 8. Illustration of carrier phase-shift variation when (a) changing phase-shift angle suddenly and (b) changing phase-shift angle gradually.

When $Err_{\rm cry} = 10$ PPM $= 10^{-5}$ and $T_s = 10^{-4}$, $\Delta\varphi_{1s}$ will be 72°. So the minimum of $f_{\rm syn}$ is

$$f_{\rm synmin} = \frac{1}{\Delta\varphi_{\rm max}/\Delta\varphi_{1s}} = 2.4 \text{ Hz}. \tag{6}$$

$f_{\rm syn}$ can be set to be 3 Hz, which means Controller 1 will send a synchronous signal to Controller 2 per 0.333 s.

3) Controller 1 sends the optimal phase-shift angle $\varphi_{\rm PWM2best}$ and $f_{\rm syn}$ to Controller 2 after calculation.

B. Synchronization Part

After calculating the optimal phase-shift angle and the synchronization frequency, both controllers will next synchronize their PWM sequences by the following steps. These processes are also shown in Fig. 6.

4) Controller 1 sends the synchronous signals to Controller 2 per 0.333 s. The synchronous signals are shown in Fig. 8(a), and they are sent out when the carrier counter of Controller 1 is zero.
5) Controller 2 saves its carrier phase-shift angle of 90° in its memory in calculation part and changes its carrier phase-shift angle gradually until its phase-shift angle become 90° upon receiving the synchronous signals.

This process should not influence other normal operation functions of inverter itself. For example, Fig. 8 shows the proper synchronization process, where Carrier 1 and Carrier 2 are the modulation carriers generated by Controller 1 and Controller 2, respectively. Before the synchronization part, the phase-shift angle between these two carriers is uncertain and it is expressed by $\varphi_{\mathrm{PWM2}} = x^{\circ}$ in Fig. 8. In Fig. 8(a), the phase shift of Carrier 2 will change suddenly when Controller 2 receives the synchronous signal at t_0. The sudden change of carrier may cause the serious output distortion because the number in carrier counter will change suddenly and this will generate the abnormal PWM commands. To avoid this problem, the carrier phase-shift angle should change gradually as shown in Fig. 8(b). In specific, when Controller 2 receives the synchronous signals, the peak value of carrier counter will change from the normal value C_{peak} (normal mode) to $C_{\mathrm{peak}} + 1$ or $C_{\mathrm{peak}} - 1$ (phase-shift mode), which will reduce or increase the carrier frequency slightly. And then φ_{PWM2} will change to $\varphi_{\mathrm{PWM2best}}$ gradually. In Fig. 8(b), the operation of reducing carrier frequency is illustrated. The formula to calculate C_{peak} is

$$C_{\mathrm{peak}} = \frac{f_{\mathrm{DSP}}}{2f_c} \tag{7}$$

where, f_{DSP} is the working frequency of DSP, for example, f_{DSP} of TMS320F28335 is 150 MHz and $f_c = 10$ kHz, C_{peak} could be derived as 7500, $C_{\mathrm{peak}} + 1 = 7501$ and $C_{\mathrm{peak}} - 1 = 7449$, respectively. So the carrier frequency deviation can be derived as

$$\frac{f_{\mathrm{DSP}}}{2\left(C_{\mathrm{peak}}+1\right)} - \frac{f_{\mathrm{DSP}}}{2C_{\mathrm{peak}}} = -1.33316 \text{ Hz} \tag{8}$$

$$\frac{f_{\mathrm{DSP}}}{2\left(C_{\mathrm{peak}}-1\right)} - \frac{f_{\mathrm{DSP}}}{2C_{\mathrm{peak}}} = 1.33351 \text{ Hz}. \tag{9}$$

When the phase-shift angle of Carrier 2 becomes 90° after t_{change}, the peak value of carrier counter of Carrier 2 will change back to C_{peak}. The t_{change} can be calculated as

$$t_{\mathrm{change}} = \frac{\left|\varphi_{\mathrm{PWM2}} - \varphi_{\mathrm{PWM2best}}\right|}{360^{\circ}} \cdot \frac{f_{\mathrm{DSP}}}{2f_c^2}. \tag{10}$$

Considering that φ_{PWM2} is uncertain, t_{change} is also uncertain. The maximum of $|\varphi_{\mathrm{PWM2}} - \varphi_{\mathrm{PWM2best}}|$ is 360°. So the maximum t_{change} is $f_{\mathrm{DSP}}/2f_c^2$. When $f_c = 10$ kHz and $f_{\mathrm{DSP}} = 150$ MHz, $t_{\mathrm{changemax}} = 0.75$ s. The time consumption of the first phase-shift operation is smaller than 0.75 s but uncertain. A better solution is to synchronize the phase-shift angle before inverters output their currents. In practice, controllers can work in advance to initialize the GSPWM when the inverters are commanded to start. After the initialization of GSPWM, the subsequent adjustments of φ_{PWM2} will be very fast and less time consuming since during each synchronization period, φ_{PWM2} will only deviate little from $\varphi_{\mathrm{PWM2best}}$.

C. Detailed Implementation Issues of Communication Channel

The novel GSPWM can employ the existing communication channels installed for the general purposes of distributed inverters, e.g., uploading the generated power information and receiving the dispatching command. The additional communication tasks for realizing GSPWM should not induce the communication jamming and increase communication investment. In this section, DSP (TMS320F28335) and RS485 communication channel are employed for explanation.

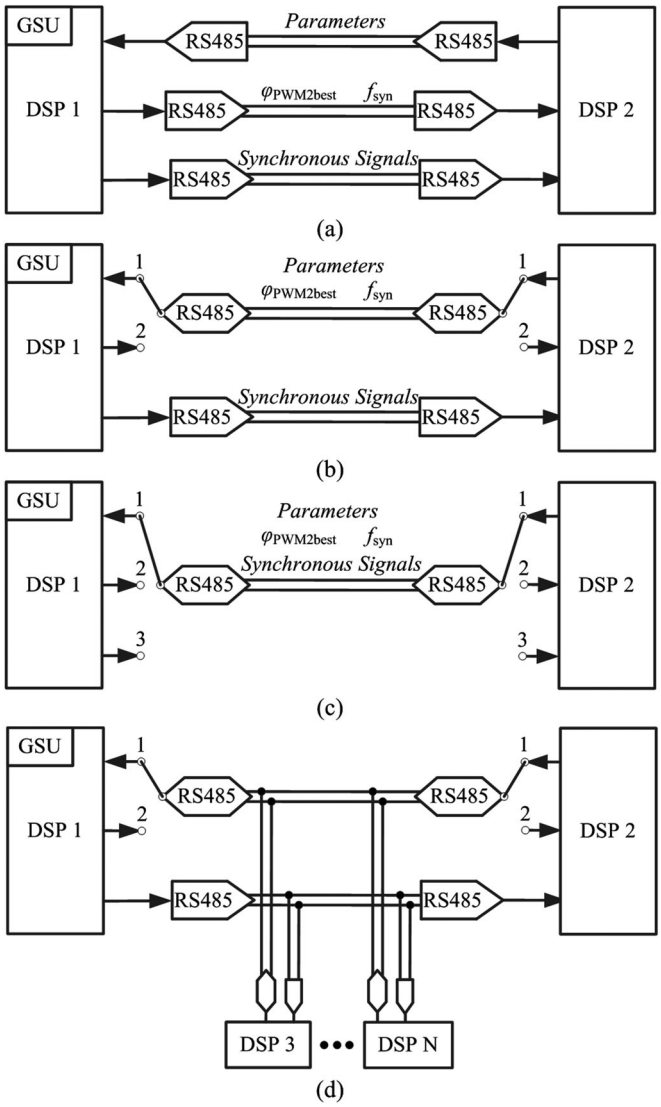

Fig. 9. Different communication structures applied in GSPWM system. (a) Three simplex communication channels. (c) One half-duplex communication channel. (c) One simplex communication channel and one half-duplex communication channel. (d) General communication structure of N inverters.

Totally, the GSU and the distributed inverters will communicate three kinds of signals, which are the parameters signals of distributed inverters sent to the GSU, calculated optimal phase-shift angles $\varphi_{\mathrm{PWM}M\mathrm{best}}$, and f_{syn} sent to the distributed inverters, synchronous signals to the distributed inverters, respectively. To effectively communicate these signals, employing three simplex communication channels is the simplest and most straightforward solution as shown in Fig. 9(a), but it is not cost-effective. Alternatively, only employing one half-duplex communication channel as shown in Fig. 9(b) is the most inexpensive solution but the corresponding communication protocol is complex. Therefore, one simplex communication channel and one half-duplex communication channel are assumed here as shown

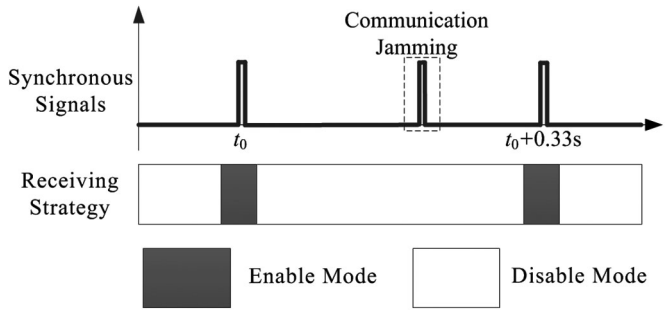

Fig. 10. Strategy to avoid communication jamming.

in Fig. 9(c). These two channels can be encapsulated into one cable. When there are N inverters, the general communication structure is shown in Fig. 9(d).

In detail, sending inverter parameters and the optimal phase-shift angles uses the protocol of serial port communication, which can avoid the communications jamming with the existing protocol and guarantee the communication accuracy. Besides, sending synchronous signals is a little bit complicated, whose detailed analysis will be presented below.

The time delay of synchronous signals in communication cable is L/c. L is the length of communication channel in meters and c is the electronic speed which is 300 000 km/s generally. $t_{dT}, t_{dR}, t_{d\mathrm{DSP1}}, t_{d\mathrm{DSP2}}$ are time delay of transmitter, receiver, DSP1 and DSP2, respectively. So the total time delay $t_{d\mathrm{total}}$ is

$$t_{d\mathrm{total}} = t_{dT} + t_{dR} + t_{d\mathrm{DSP1}} + t_{d\mathrm{DSP2}} + L \times 3.33 \text{ ns}. \quad (11)$$

So the angular deviation caused by time delay is

$$360^\circ \cdot \frac{t_{d\mathrm{total}}}{1/f_c} = 360^\circ f_c t_{d\mathrm{total}}. \quad (12)$$

According to the datasheet of RS485, the typical time delays of transmitter and receiver are 30 and 90 ns, respectively, and the maximum time delays of them are 60 and 200 ns, respectively. According to the datasheet of TMS320F28335, the working frequency is 150 MHz and the maximum sending and receiving time delay is 6.67 ns. So the total typical and maximum time delays are

$$t_{d\mathrm{totaltyp}} = 133.3 \text{ ns} + L \times 3.33 \text{ ns} \quad (13)$$

$$t_{d\mathrm{totalmax}} = 273.3 \text{ ns} + L \times 3.33 \text{ ns}. \quad (14)$$

For example, when $f_c = 10$ kHz and the length of communication cable is 100 m, the typical angular deviation caused by time delay can be derived as 2.18° according to (12). The phase angle deviation caused by the communication time delay, especially that induced by the communication cable, can be compensated by simply adjusting the algorithm in distributed inverters when knowing the communication distance.

Additionally, communication jamming of synchronous signals may cause the wrong synchronization operation. To avoid this problem, the digital controller adopts the specially designed receiving strategy, which is illustrated in Fig. 10. In specific, the DSPs in distributed inverters have known f_{syn} since it is sent out with the optimal phase-shift angle together. So DSPs can calculate arrival time of synchronous signals roughly. DSP will work at enable mode to receive synchronous signals according to the roughly calculated arrival time. The duration of enable mode should guarantee the synchronous signals can be received and the communication jamming signals can be ignored.

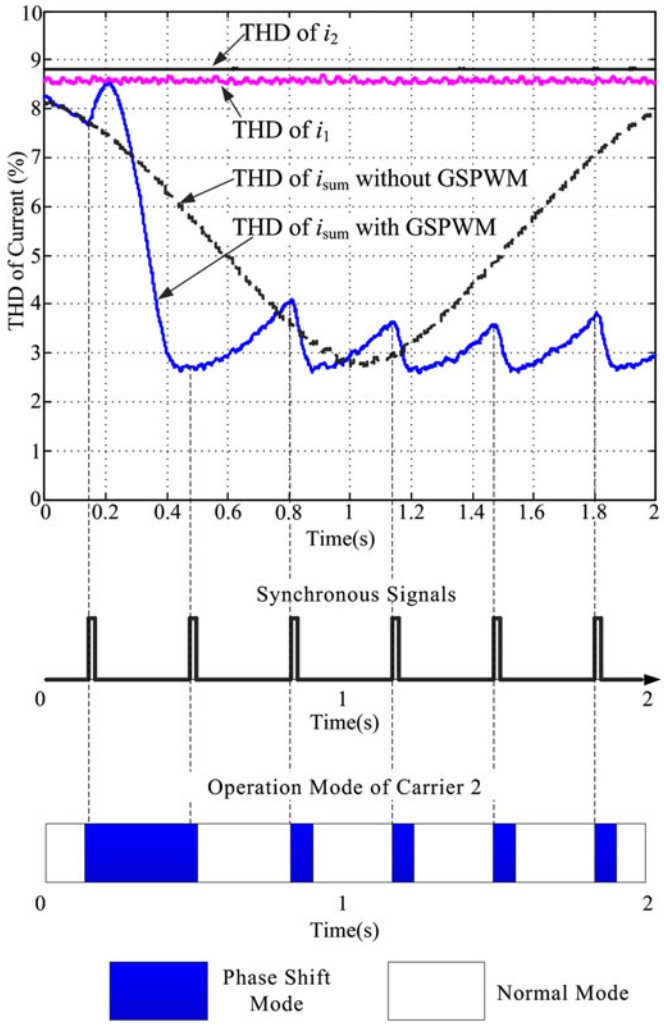

Fig. 11. Simulation result of THDs, synchronous signals and operation mode of Carrier 2.

GSPWM will calculate the optimal phase-shift angles and f_{syn} at a very low frequency since the inverter parameters will not change rapidly. And synchronous signals will be periodically sent out according to the calculated sending frequency f_{syn}.

Fig. 11 shows the simulation result of current THDs, synchronous signals, and operation mode of Carrier 2 within 2 s when employing GSPWM at 0.13 s under the same operation conditions as listed in Table I. The operation mode of Carrier 2 will change from normal mode to phase-shift mode when Controller 2 receives the synchronous signals and it will change back to normal mode when $\varphi_{\mathrm{PWM2}} = \varphi_{\mathrm{PWM2best}} = 90^\circ$. The f_{syn} is set to be 3 Hz and the THD of i_{sum} is lower than 5% as expected.

III. Calculation Method of GSPWM Under Complex Working Condition

When the inverters connected to the same PCC work under the same condition, the optimal phase-shift angles among them can be easily calculated. But when the distributed inverters

work under different conditions including different dc-link voltages, different switching frequencies, different output filters, and different feeder impedances, it is difficult to find the optimal phase-shift angles and the synchronous frequency. This section will then elaborate a method to calculate the optimal phase-shift angles and the synchronous frequency under the complicated working conditions.

In detail, i_{M} and i_{hM} can be expressed as

$$i_M = i_{1M} + i_{\mathrm{hM}} \tag{15}$$

$$i_{\mathrm{hM}} = \sum_{f=f_{1M}+1}^{\infty} i_{\mathrm{hMf}}. \tag{16}$$

And the RMS value of i_{M} and i_{hM} can be written as

$$I_M = \sqrt{I_{1M}^2 + I_{\mathrm{hM}}^2} \tag{17}$$

$$I_{\mathrm{hM}} = \sqrt{\sum_{f=f_{1M}+1}^{\infty} I_{\mathrm{hMf}}^2}. \tag{18}$$

The THD of i_{M} can be written as

$$\mathrm{THD}_M = \sqrt{I_{\mathrm{hM}}^2 / I_{1M}^2}. \tag{19}$$

And the total current and its fundamental and total harmonic parts as well as the specific harmonic current can be written as

$$i_{\mathrm{sum}} = \sum_{M=1}^{N} i_M = \sum_{M=1}^{N} (i_{1M} + i_{\mathrm{hM}}) = i_{1\mathrm{sum}} + i_{h\mathrm{sum}} \tag{20}$$

$$i_{1\mathrm{sum}} = \sum_{M=1}^{N} i_{1M} \tag{21}$$

$$i_{h\mathrm{sum}} = \sum_{M=1}^{N} i_{\mathrm{hM}} \tag{22}$$

$$i_{h\mathrm{sum}f} = \sum_{M=1}^{N} i_{\mathrm{hMf}}. \tag{23}$$

The RMS values of $i_{\mathrm{sum}}, i_{1\mathrm{sum}}, i_{h\mathrm{sum}}, i_{h\mathrm{sum}f}$ can be derived as

$$I_{\mathrm{sum}} = \sqrt{I_{1\mathrm{sum}}^2 + I_{h\mathrm{sum}}^2} \tag{24}$$

$$I_{1\mathrm{sum}} = \sqrt{\sum_{M=1}^{N} I_{1M}^2} \tag{25}$$

$$I_{h\mathrm{sum}} = \sqrt{\sum_{f=f_{1M}+1}^{\infty} I_{h\mathrm{sum}f}^2} = F\left(\varphi_{\mathrm{PWM}1}, \ldots, \varphi_{\mathrm{PWM}N}\right) \tag{26}$$

$$I_{h\mathrm{sum}f} = W_1\left(\varphi_{\mathrm{PWM}1}, \ldots, \varphi_{\mathrm{PWM}N}\right) \tag{27}$$

where, F and W_1 are functions of $\varphi_{\mathrm{PWM}M}$. The THD of i_{sum} is

$$\mathrm{THD}_{\mathrm{sum}} = \sqrt{I_{h\mathrm{sum}}^2 / I_{1\mathrm{sum}}^2}. \tag{28}$$

The goal of GSPWM is to minimize $\mathrm{THD}_{\mathrm{sum}}$. GSPWM will not change $I_{1\mathrm{sum}}$ but it can change $I_{h\mathrm{sum}}$ in (28). In detail, Controller 1 receives the parameters sent from Controller *M* (*M* = 2, . . . , *N*) including the dc bus voltage $U_{\mathrm{dc}M}$, the sum of filter inductance and feeder inductance L_{M}, the switching frequency f_{cM}, the active power P_{M} and the reactive power Q_{M}. The GSU function will then begin its three main tasks.

1) GSU generates the formula of $I_{h\mathrm{sum}} = F(\varphi_{\mathrm{PWM}1,\ldots}, \varphi_{\mathrm{PWM}N})$ to express the relationship between the phase-shift angle $\varphi_{\mathrm{PWM}M}$ and the RMS value of harmonic current $I_{h\mathrm{sum}}$ by using the double integral Fourier analysis.
2) GSU calculates the optimal phase-shift angle $\varphi_{\mathrm{PWM}M\mathrm{best}}$ to minimize $I_{h\mathrm{sum}}$ by using the intelligent optimization algorithms.
3) GSU calculates the sending frequency f_{syn} of synchronous signals by using $I_{h\mathrm{sum}} = F(\varphi_{\mathrm{PWM}1,\ldots}, \varphi_{\mathrm{PWM}N})$ and the intelligent optimization algorithms.

GSU will repeat the above three main tasks under a very low frequency because the corresponding parameters of distributed inverters will not change rapidly.

A. Mathematical Relationship Between $\varphi_{\mathrm{PWM}M}$ and RMS Value of Total Harmonic Current $i_{h\mathrm{sum}}$

The double integral Fourier analysis provides a mathematically rigorous method for studying PWM characteristics in the frequency domain [22]. The current harmonics will demonstrate different characteristics when employing different inverter types (single-phase inverter, three-phase inverter, multilevel inverter, etc.), different modulation modes (continuous PWM, discontinuous PWM, SVPWM, etc.) and different filter types (*L*, *LC*, or *LCL*). Holmes and Lipo [23] have proposed formulas to represent current harmonics in the frequency domain by considering different inverter types and modulation modes. The current harmonics can be represented with a general formula as (16), where the phasor of i_{hMf} can be expressed as

$$\dot{I}_{\mathrm{hMf}} = I_{\mathrm{hMf}} e^{j\varphi_{\mathrm{hMf}}} \tag{29}$$

where I_{hMf} and φ_{hMf} are the RMS value and angle of $\dot{I}_{\mathrm{hMf}}$, respectively. GSPWM does not change I_{hMf}, but it can change φ_{hMf}. So φ_{hMf} can be expressed as

$$\varphi_{\mathrm{hMf}} = G_{\mathrm{Mf}}\left(\varphi_{\mathrm{PWM}1}, \ldots, \varphi_{\mathrm{PWM}N}\right). \tag{30}$$

When i_{hM} flows to PCC, the current harmonics with the same frequency are summed and the summed value is determined by their phases and amplitudes

$$\begin{aligned} \dot{I}_{h\mathrm{sum}f} &= I_{h\mathrm{sum}f} e^{j\varphi_{h\mathrm{sum}f}} = \sum_{M=1}^{N} I_{\mathrm{hMf}} e^{j\varphi_{\mathrm{hMf}}} \\ &= \sum_{M=1}^{N} I_{\mathrm{hMf}} e^{jG_{\mathrm{Mf}}(\varphi_{\mathrm{PWM}1},\ldots,\varphi_{\mathrm{PWM}N})} \\ &= W_f\left(\varphi_{\mathrm{PWM}1}, \ldots, \varphi_{\mathrm{PWM}N}\right) \end{aligned} \tag{31}$$

$$\begin{aligned} I_{h\mathrm{sum}f} &= \left| \sum_{M=1}^{N} I_{\mathrm{hMf}} e^{j\varphi_{\mathrm{hMf}}} \right| \\ &= W_{1f}\left(\varphi_{\mathrm{PWM}1}, \ldots, \varphi_{\mathrm{PWM}N}\right) \end{aligned} \tag{32}$$

$$\begin{aligned}\varphi_{h\mathrm{sum}f} &= \operatorname{angle}\left(\sum_{M=1}^{N} I_{\mathrm{hM}f} e^{j\varphi_{\mathrm{hM}f}}\right)\\ &= W_{2f}\left(\varphi_{\mathrm{PWM}1},\ldots,\varphi_{\mathrm{PWM}N}\right)\end{aligned} \tag{33}$$

where, W_f, W_{1f}, W_{2f} are functions of $\varphi_{\mathrm{PWM}M}$, and they could have different specific expression when different inverter types and modulation modes are employed. And they can be calculated by double integral Fourier analysis method with the known inverter parameters. So the relationship between $I_{h\mathrm{sum}}$ and $\varphi_{\mathrm{PWM}M}$ can be generally expressed as

$$\begin{aligned}I_{h\mathrm{sum}} &= \sqrt{\sum_{f=f_{1M}+1}^{\infty} I_{h\mathrm{sum}f}^2}\\ &= \sqrt{\sum_{f=f_{1M}+1}^{\infty}\left|\sum_{M=1}^{N} I_{\mathrm{hM}f} e^{j\varphi_{\mathrm{hM}f}}\right|^2}\\ &= F\left(\varphi_{\mathrm{PWM}1},\ldots,\varphi_{\mathrm{PWM}N}\right).\end{aligned} \tag{34}$$

In the following, single-phase inverter with unipolar modulation mode is employed as an example to express this calculation method in detail. When using the unipolar modulation mode and *L* filter for single-phase inverters, the output voltage harmonics of inverter *M* are

$$u_{\mathrm{hM}} = \frac{4U_{\mathrm{dc}M}}{\pi}\sum_{k_M=1}^{\infty}\sum_{\substack{n_M=-\infty\\ n_M\neq 0}}^{\infty}\left\{\begin{array}{c}\dfrac{1}{2k_M}\cdot J_{2n_M-1}\left(2m_M k_M\dfrac{\pi}{2}\right)\\ \cdot\sin\left(\left[2k_M+\left[2n_M-1\right]\right]\dfrac{\pi}{2}\right)\\ \cdot\cos\left(2k_M\omega_{\mathrm{cM}}t+\left[2n_M-1\right]\omega_{1M}t\right)\end{array}\right\} \tag{35}$$

where, $\omega_{\mathrm{cM}}=2\pi f_{\mathrm{cM}}, \omega_{1M}=2\pi f_{1M}. U_{\mathrm{dc}M}, f_{\mathrm{cM}}, f_{1M}$ are dc bus voltage, switching frequency, fundamental frequency of inverter *M*, respectively. k_{M} and n_{M} are multiple of switching frequency and multiple of fundamental frequency of inverter *M*, respectively. $J_n(x)$ is Bessel function

$$J_n(x)=\sum_{j=1}^{\infty}\frac{(-1)^j x^{2j+n}}{2^{2j+n} j!\,(n+j)!}. \tag{36}$$

Assuming the grid voltage is purely sinusoidal, for inverter with only single inductor filter,

$$u_{\mathrm{hM}} = L_M\frac{di_{\mathrm{hM}}}{dt} \tag{37}$$

where, L_{M} is the sum of filter inductance and feeder inductance. So the output high-frequency current harmonics are

$$i_{\mathrm{hM}} = \sum_{k_M=1}^{\infty}\sum_{\substack{n_M=-\infty\\ n_M\neq 0}}^{\infty}\left\{\begin{array}{c}\sqrt{2}\cdot I_{hM(k_M f_{\mathrm{cM}}+n_M f_{1M})}\\ \cdot\cos\left(-90^\circ+2k_M\omega_{\mathrm{cM}}t+\left[2n_M-1\right]\omega_{1M}t\right)\end{array}\right\} \tag{38}$$

where

$$I_{\mathrm{hM}f} = I_{hM(k_M f_{\mathrm{cM}}+n_M f_{1M})} = \left\{\begin{array}{c}\dfrac{u_{\mathrm{dc}M}}{L_M}\cdot\dfrac{2\sqrt{2}}{\pi}\cdot\dfrac{1}{2k_M\omega_{\mathrm{cM}}+\left[2n_M-1\right]\omega_{1M}}\\ \cdot\dfrac{1}{2k_M}\cdot J_{2n_M-1}\left(2m_M k_M\dfrac{\pi}{2}\right)\\ \cdot\sin\left(\left[2k_M+\left[2n_M-1\right]\right]\dfrac{\pi}{2}\right)\end{array}\right\}. \tag{39}$$

When N inverters connect to the same PCC, the harmonic current flowing from inverter M to PCC is

$$i_{\mathrm{hM}} = \sum_{k_M=1}^{\infty}\sum_{\substack{n_M=-\infty\\ n_M\neq 0}}^{\infty}\left\{\begin{array}{c}\sqrt{2}\cdot I_{hM(k_M f_{\mathrm{cM}}+n_M f_{1M})}\\ \cdot\cos\left(\begin{array}{c}-90^\circ+2k_M\left[\omega_{\mathrm{cM}}t+\varphi_{\mathrm{PWM}M}\right]\\ +\left[2n_M-1\right]\left[\omega_{1M}t+\varphi_{1M}\right]\end{array}\right)\end{array}\right\} \tag{40}$$

$$\begin{aligned}\varphi_{\mathrm{hM}f} &= \varphi_{hM(k_M f_{\mathrm{cM}}+n_M f_{1M})}\\ &= G_{\mathrm{M}f}\left(\varphi_{\mathrm{PWM}1},\ldots,\varphi_{\mathrm{PWM}N}\right)\\ &= -90^\circ+2k_M\varphi_{\mathrm{PWM}M}+\left[2n_M-1\right]\varphi_{1M}\end{aligned} \tag{41}$$

where, φ_{1M} is the phase-shift angle between fundamental voltage of inverter M and fundamental voltage of inverter 1, and φ_{1M} will not change when using GSPWM. When i_{hM} flows to PCC, the current harmonics with the same frequency are summed and the summed value is determined by their phases and amplitudes. When the switching frequencies and modulation mode of inverters are consistent, $k_{\mathrm{M}}, n_{\mathrm{M}}$ can be replaced by *k*, *n*. Then using equations (31)–(33), equation (34) can be further expressed as (42) as shown bottom of the page.

In the general case, the switching frequencies and modulation mode of inverters are different, $I_{h\mathrm{sum}}$ and $\varphi_{\mathrm{hM}f}$ can be expressed

$$I_{h\mathrm{sum}} = \sqrt{\sum_{k=1}^{\infty}\sum_{\substack{n=-\infty\\ n\neq 0}}^{\infty}\left|\sum_{M=1}^{N}\left\{\begin{array}{c}I_{\mathrm{hM}(\mathrm{k_M f_{cM}+n_M f_{1M}})}\\ \cdot e^{j(-90^\circ+2k\varphi_{\mathrm{PWM}M}+[2n-1]\varphi_{1M})}\end{array}\right\}\right|^2} = F\left(\varphi_{\mathrm{PWM}1},\ldots,\varphi_{\mathrm{PWM}N}\right) \tag{42}$$

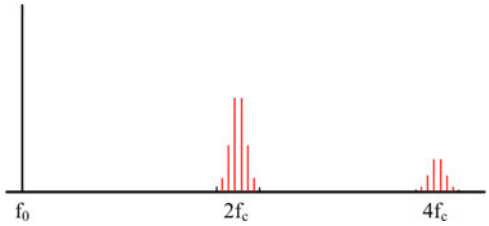

Fig. 12. Output current spectrum of single-phase inverter when using the unipolar modulation mode.

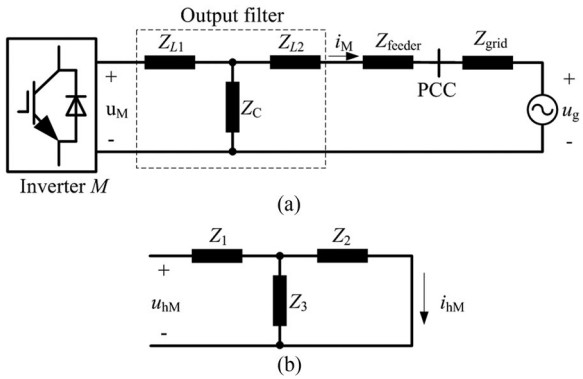

Fig. 13. General output circuit of inverter. (a) Equivalent output circuit. (b) Simplified output circuit.

as

$$I_{h\mathrm{sum}} = \sqrt{\sum_{f=f_{1M}+1}^{\infty}\left|\sum_{M=1}^{N} I_{\mathrm{hMf}} e^{j\varphi_{\mathrm{hMf}}}\right|^2} = F\left(\varphi_{\mathrm{PWM1}},\ldots,\varphi_{\mathrm{PWM}N}\right) \quad (43)$$

$$\varphi_{\mathrm{hMf}} = \theta_{\mathrm{hMf}} + 2k_M\varphi_{\mathrm{PWM}M} + \left[2n_M - 1\right]\varphi_{1M}. \quad (44)$$

Equation (43) represents the general expression of $I_{h\mathrm{sum}} = F(\varphi_{\mathrm{PWM1},\ldots},\varphi_{\mathrm{PWM}N})$ to express the relationship between $\varphi_{\mathrm{PWM}M}$ and $I_{h\mathrm{sum}}$. The calculation result is accurate if all harmonics are involved in (44). But such accurate calculation costs too much time in practice. Considering the tradeoff between calculation time and accuracy, only main harmonics are involved in (43). For single-phase inverters with unipolar modulation mode, only harmonics with frequency $2k_{\mathrm{M}}f_{\mathrm{cM}} + [2n_{\mathrm{M}} - 1]f_{1M}\,(k_{\mathrm{M}} = 1, 2; n_{\mathrm{M}} = 1, 2, 3)$ are involved as shown in Fig. 12.

When further considering the feeder parameters, the parasitic components and the different filter types, the analysis procedure is similar to the above presentation. But the equations (35)–(41) can only be used to calculate I_{hMf} and φ_{hMf} for the inverter with single *L* filter because $\theta_{\mathrm{hMf}} = -90°$ in (38), (40), and (41). More general expressions for various filter types are demonstrated below. Fig. 13(a) shows the general output circuit which apply to *L* filter, *LC* filter, and *LCL* filter. And the feeder parameters and the parasitic components can be taken into consideration. Z_{L1}, Z_{L2}, Z_C are determined by the output filter and Table II shows their values.

Assuming the grid voltage u_g is purely sinusoidal, so the output circuit can be simplified as Fig. 13(b). In this simplified circuit

TABLE II
PARAMETERS OF DIFFERENT FILTER TYPE

Filter	Z_{L1}	Z_{L2}	Z_C
L	$r_L + \mathrm{jwL}$	0	∞
LC	$r_L + \mathrm{jwL}$	0	$r_C + 1/\mathrm{jwC}$
LCL	$r_{L1} + \mathrm{jwL}_1$	$r_{L2} + \mathrm{jwL}_2$	$r_C + 1/\mathrm{jwC}$

$$Z_1 = Z_{L1} \quad (45)$$

$$Z_2 = Z_{L2} + Z_{\mathrm{feeder}} + Z_{\mathrm{grid}} \quad (46)$$

$$Z_3 = Z_c. \quad (47)$$

Z_1, Z_2, Z_3 are the functions of *f*. The current phasor $\dot{I}_{\mathrm{hMf}}$ can be written as

$$\dot{I}_{\mathrm{hMf}} = \dot{U}_{\mathrm{hMf}}\frac{Z_3}{Z_1Z_2 + Z_1Z_3 + Z_2Z_3}. \quad (48)$$

The RMS value and angle of $\dot{I}_{\mathrm{hMf}}$. is

$$I_{\mathrm{hMf}} = \left|\dot{U}_{\mathrm{hMf}}\frac{Z_3}{Z_1Z_2 + Z_1Z_3 + Z_2Z_3}\right| \quad (49)$$

$$\varphi_{\mathrm{hMf}} = \theta_{\mathrm{hMf}} + 2k_M\varphi_{\mathrm{PWM}M} + \left[2n_M - 1\right]\varphi_{1M} \quad (50)$$

where

$$\theta_{\mathrm{hMf}} = \mathrm{angle}\left(\frac{Z_3}{Z_1Z_2 + Z_1Z_3 + Z_2Z_3}\right). \quad (51)$$

Equations (45) to (51) can be used to calculate I_{hMf} and φ_{hMf} for the inverter with any kinds of filter. I_{hMf} and φ_{hMf} are then used to calculate $I_{h\mathrm{sum}}$ in (43).

B. Intelligent Optimization Algorithms to Determine Phase-Shift Angle $\varphi_{\mathrm{PWM}M}$

Using Euler formula, (34) can be revised as

$$I_{h\mathrm{sum}} = \sqrt{\sum_{f=0}^{\infty}\left(\sum_{M=1}^{N} I_{\mathrm{hMf}}\cos\left(\varphi_{\mathrm{hMf}}\right)\right)^2 + \sum_{f=0}^{\infty}\left(\sum_{M=1}^{N} I_{\mathrm{hMf}}\sin\left(\varphi_{\mathrm{hMf}}\right)\right)^2} = F\left(\varphi_{\mathrm{PWM1}},\ldots,\varphi_{\mathrm{PWM}N}\right). \quad (52)$$

The objective is to find the minimum value of $I_{h\mathrm{sum}} = F(\varphi_{\mathrm{PWM1}}\ldots\ldots\varphi_{\mathrm{PWM}N})$, which is subject to $0° \le \varphi_{\mathrm{PWM}M} \le 360°$, for $M = 1,\ldots,N$.

It is hard to find $\varphi_{\mathrm{PWM}M\mathrm{best}}$ to minimize $I_{h\mathrm{sum}}$ through the traditional mathematical methods because this is a large-scale nonlinear optimization problem. Particle swarm optimization (PSO) method is used widely for the optimization of continuous nonlinear functions [24]–[26], and it is employed here to find $\varphi_{\mathrm{PWM}M\mathrm{best}}$.

PSO is an evolutionary computation technique [24], [25]. It uses many particles that fly through the problem hyperspace with the given velocities. Fig. 14 shows the principle of PSO. In each iteration step, the velocities of particles are adjusted according to the historical best position of the particle itself and

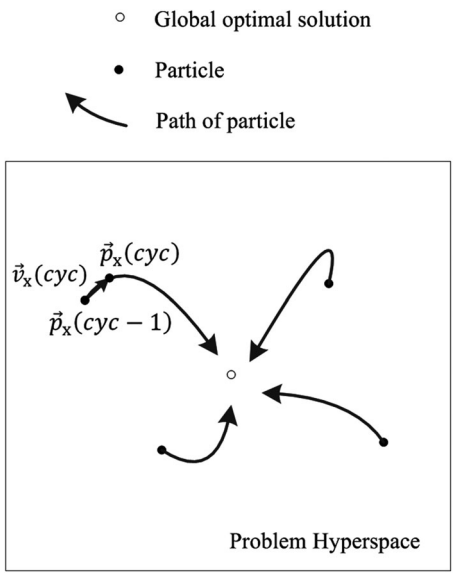

Fig. 14. Principle illustration of PSO.

the historical best position of all particles. The movement of each particle naturally evolves to an optimal or near-optimal solution [26].

In the real number space, the number of particles is $X_{\max}$. The position of each particle x (x = 1,2,..., $X_{\max}$) can be determined by vector $\vec{p}_x \in R^n$ and its velocity is $\vec{v}_x \in R^n$ [27]. The iteration formula is

$$\vec{p}_x\left(cyc\right) = \vec{p}_x\left(cyc-1\right) + \vec{v}_x\left(cyc\right) \tag{53}$$

where, *cyc* refers to the cycle index of PSO. Assuming the historical best position of particle x is $\vec{p}_{x\mathrm{best}}$ and the historical best position of all particles is $\vec{p}_{g\mathrm{best}}$. The velocities of each particle are related to $\vec{p}_{x\mathrm{best}}$ and $\vec{p}_{g\mathrm{best}}$. Since the relative importance of these two factors can vary from one decision to another, it is reasonable to apply random weights to each part. So the iteration formula of velocity is

$$\vec{v}_x\left(cyc\right) = \left\{ \begin{array}{c} \vec{v}_x\left(cyc-1\right) \\ +\, c_1 \cdot r\mathrm{and}_1\left([0,1]\right) \cdot \left(\vec{p}_{x\mathrm{best}} - \vec{p}_x\left(cyc-1\right)\right) \\ +\, c_2 \cdot r\mathrm{and}_2\left([0,1]\right) \cdot \left(\vec{p}_{g\mathrm{best}} - \vec{p}_x\left(cyc-1\right)\right) \end{array} \right\} \tag{54}$$

where, c_1 and c_2 are two positive numbers and $r\mathrm{and}_1$ and $r\mathrm{and}_2$ are two random numbers with uniform distribution in the range [0, 1]. As suggested in [28], the proper starting point is $c_1 = c_2 = 2$.

When PSO is applied to calculate optimal phase shifts, the range of $\varphi_{\mathrm{PWM}M}$ is from 0° to 360°. The position and velocity of each particle x (x = 1,2,..., $X_{\max}$) at cycle index *cyc* are $\vec{\varphi}_{\boldsymbol{x}}\left(cyc\right)$ and $\vec{v}_x\left(cyc\right)$ which are defined as

$$\begin{aligned} \vec{\varphi}_x\left(cyc\right) &= \left[\varphi_{\mathrm{PWM}2x}\left(cyc\right), \varphi_{\mathrm{PWM}3x}\left(cyc\right), \ldots\ldots, \right. \\ &\quad \left. \varphi_{\mathrm{PWM}Nx}\left(cyc\right)\right] \end{aligned} \tag{55}$$

$$\begin{aligned} \vec{v}_x\left(cyc\right) &= \left[v_{\mathrm{PWM}2x}\left(cyc\right), v_{\mathrm{PWM}3x}\left(cyc\right), \ldots\ldots, \right. \\ &\quad \left. v_{\mathrm{PWM}Nx}\left(cyc\right)\right]. \end{aligned} \tag{56}$$

$\varphi_{\mathrm{PWM}Mx}(cyc)$ is the phase-shift angle of inverter M in particle x at cycle index *cyc*. $v_{\mathrm{PWM}Mx}(cyc)$ is the change velocity of $\varphi_{\mathrm{PWM}Mx}(cyc)$. $\vec{\varphi}_{\boldsymbol{x}}\left(cyc\right)$ and $\vec{v}_{\boldsymbol{x}}\left(cyc\right)$ do not contain $\varphi_{\mathrm{PWM}1x}$ and $v_{\mathrm{PWM}1x}$, because $\varphi_{\mathrm{PWM}1x}$ and $v_{\mathrm{PWM}1x}$ are 0. The dimensions of $\vec{\varphi}_{\boldsymbol{x}}\left(cyc\right)$ and $\vec{v}_{\boldsymbol{x}}\left(cyc\right)$ are both N-1, and $\vec{\varphi}_{\boldsymbol{x}}\left(cyc\right)$ needs to be calculated to find minimum $I_{h\mathrm{sum}}$. According to the above theory, the processes of particle swarm methodology are to

1) Initialize the positions and velocities of particles randomly in the problem hyperspace. For particle x (x = 1,2,..., $X_{\max}$), its initialized random position is $\vec{\varphi}_x\left(0\right)$($x$ = 1,2,..., $X_{\max}$) and initialized random velocity is $\vec{v}_x\left(0\right)$(x = 1,2,..., $X_{\max}$)

$$\vec{\varphi}_x\left(0\right) = \left[\begin{array}{l} \varphi_{\mathrm{PWM2x}}\left(0\right) = r\mathrm{and}\left([0°, 360°]\right), \\ \varphi_{\mathrm{PWM3x}}\left(0\right) = r\mathrm{and}\left([0°, 360°]\right), \\ \qquad \ldots\ldots, \\ \varphi_{\mathrm{PWM}N\mathrm{x}}\left(0\right) = r\mathrm{and}\left([0°, 360°]\right) \end{array} \right] \tag{57}$$

$$\vec{v}_x\left(0\right) = \left[\begin{array}{l} v_{\mathrm{PWM2}x}\left(0\right) = v_{\max} \cdot r\mathrm{and}\left([-1,1]\right), \\ v_{\mathrm{PWM3}x}\left(0\right) = v_{\max} \cdot r\mathrm{and}\left([-1,1]\right), \\ \qquad \ldots\ldots, \\ v_{\mathrm{PWM}Nx}\left(0\right) = v_{\max} \cdot r\mathrm{and}\left([-1,1]\right) \end{array} \right] \tag{58}$$

where rand([0° to 360°]) is the random phase-shift angle, $v_{\max}$ is the maximum velocity and initialized cycle index $cyc = 0$.

2) Calculate $I_{h\mathrm{sum}}$ of each particle with (52):

$$\begin{aligned} I_{h\mathrm{sum}x}\left(cyc\right) &= F\left(\varphi_{\mathrm{PWM1}x}\left(cyc\right) = 0, \vec{\varphi}_x\left(cyc\right)\right) \\ x &= 1, 2, \ldots, X_{\max} \end{aligned} \tag{59}$$

where, $I_{h\mathrm{sum}x}(cyc)$ is the specific $I_{h\mathrm{sum}}$ value at position $\vec{\varphi}_{\boldsymbol{x}}\left(cyc\right)$. Then the algorithm records the historical best position of particle x as $\vec{\varphi}_{x\mathrm{best}}$ and $I_{h\mathrm{sum}}$ is the minimum value of historical values of particle x at position $\vec{\varphi}_{x\mathrm{best}}$

$$\begin{aligned} F\left(0, \vec{\varphi}_{x\mathrm{best}}\right) &= \min\left(F\left(0, \vec{\varphi}_x\left(cyc_h\right)\right)\right) \\ cyc_h &= 0, \ldots, cyc \end{aligned} \tag{60}$$

where, cyc_h is the historical cycle index. The algorithm records the historical best position of all particles as $\vec{\varphi}_{g\mathrm{best}}$ and $I_{h\mathrm{sum}}$ is the minimum value of historical values of all particles at position $\vec{\varphi}_{g\mathrm{best}}$

$$\begin{aligned} F\left(0, \vec{\varphi}_{g\mathrm{best}}\right) &= \min\left(F\left(0, \vec{\varphi}_{x\mathrm{best}}\right)\right) \\ x &= 1, 2, \ldots, X_{\max}. \end{aligned} \tag{61}$$

3) Increase *cyc* by 1. Update the velocities positions of all particles and the iteration formula as

$$\vec{v}_{\mathrm{x}}\left(cyc\right) = \left\{ \begin{array}{c} \vec{v}_x\left(cyc-1\right) \\ +c_1 \cdot r\mathrm{and}_1\left([0,1]\right) \cdot \left(\vec{\varphi}_{x\mathrm{best}} - \vec{\varphi}_x\left(cyc-1\right)\right) \\ +c_2 \cdot r\mathrm{and}_2\left([0,1]\right) \cdot \left(\vec{\varphi}_{g\mathrm{best}} - \vec{\varphi}_x\left(cyc-1\right)\right) \end{array} \right\} \tag{62}$$

$$\vec{\varphi}_x\left(cyc\right) = \vec{\varphi}_x\left(cyc-1\right) + \vec{v}_x\left(cyc\right). \tag{63}$$

Then repeat 2) and 3) until $cyc > cyc_{\max}$. $cyc_{\max}$ is the maximum cycle index.

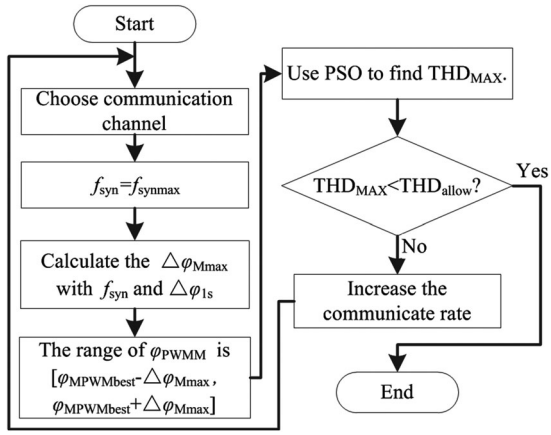

Fig. 15. Flow chart of finding the optimal solution of $f_{\rm syn}$.

4) The optimal solution is $\vec{\varphi}_{g\rm best}$

$$\vec{\varphi}_{g\rm best}=[\varphi_{\rm PWM2best},\varphi_{\rm PWM3best},\ldots,\varphi_{{\rm PWM}N{\rm best}}]. \quad (64)$$

C. Determine the Minimum Synchronous Signals' Frequency $f_{\rm synmin}$

When there are only two inverters with the same parameters, the method to calculate $f_{\rm synmin}$ is shown in Section II-A. This method is inappropriate when many inverters have different parameters, because the change rules of phase-shift angle of each inverter are unknown. It is hard to calculate $\Delta\varphi_{M\max}$ with the predefined maximum allowed THD, but it is convenient to calculate the maximum THD with the known $\Delta\varphi_{M\max}$. Therefore, it can be realized by presetting the synchronous frequency and examining $\Delta\varphi_{M\max}$ and the maximum THD appeared. Doing so, the synchronous frequency can be determined according to the allowed maximum communication speed. Above calculation is also realized by PSO. Compared with that presented in Section III-B, the differences between them are that the range of $\varphi_{{\rm PWM}M}$ is from $\varphi_{{\rm PWM}M{\rm best}}-\Delta\varphi_{M\max}$ to $\varphi_{{\rm PWM}M{\rm best}}+\Delta\varphi_{M\max}$ instead of 0°–360° and the calculation purpose is to find the maximum THD instead of the minimum THD and $\varphi_{{\rm PWM}M{\rm best}}$. So this problem can be expressed as follows.

Find the maximum of an objective function $I_{h\rm sum}=F(\varphi_{\rm PWM1}.....\varphi_{{\rm PWM}N})$

Subject to

$\varphi_{{\rm PWM}M{\rm best}}-\Delta\varphi_{M\max}\le\varphi_{{\rm PWM}M}\le\varphi_{{\rm PWM}M{\rm best}}+\Delta\varphi_{M\max}$, for $M=1,\ldots,N$where $\varphi_{{\rm PWM}M{\rm best}}$ is the result in Section III-B and $\Delta\varphi_{M\max}$ is calculated with $f_{\rm syn}$ and $\Delta\varphi_{1s}$ proposed in Section II.

The processes are to:

1) choose communication channel. Let $f_{\rm syn}=f_{\rm synmax}$, and $f_{\rm synmax}$ is the maximum sending frequency of synchronous signals with the chosen communication channel;
2) calculate $\Delta\varphi_{M\max}$ with $f_{\rm syn}$ and $\Delta\varphi_{1s}$;
3) use PSO in Section III-B to find the maximum THD when the range of $\varphi_{{\rm PWM}M}$ is from $\varphi_{{\rm PWM}M{\rm best}}-\Delta\varphi_{M\max}$ to $\varphi_{{\rm PWM}M{\rm best}}+\Delta\varphi_{M\max}$;
4) if the maximum THD is lower than maximum allowed THD, the communication channel meets the requirement. If not, increase the communicate rate and repeat 1).

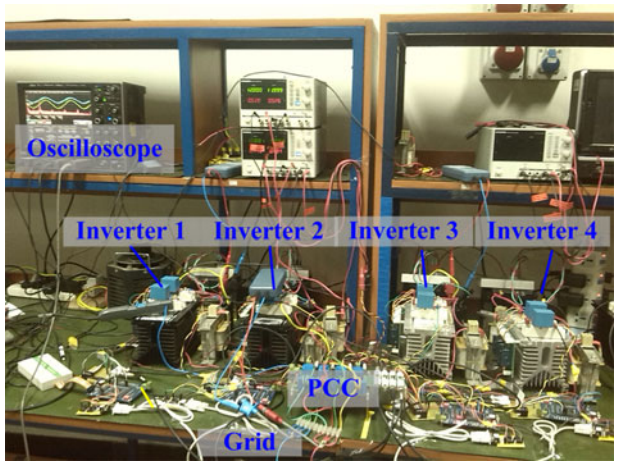

Fig. 16. Photograph of experimental prototype.

The flow chart of these processes is illustrated in Fig. 15.

In summary, the whole processes of general GSPWM includes calculation part and synchronization part, where:

1) each inverter sends its parameters to GSU;
2) GSU calculates the $\varphi_{{\rm PWM}M{\rm best}}$;
3) GSU calculates the $f_{\rm syn}$;
4) GSU sends $\varphi_{{\rm PWM}M{\rm best}}$ and $f_{\rm syn}$ to inverter M;
5) GSU sends synchronous signals to inverters periodically;
6) controller changes its carrier phase shift angle gradually until its phase shift angle becomes the calculated best value upon receiving the synchronous signals.

To reduce the calculation burden, calculation part is divided into two modes: 1) *First Calculation Mode* which operates at the first time and 2) *General Calculation Mode*.

1) First Calculation Mode: To finish the first time phase-shift operation before inverters output their quantities, inverters will send their rated parameters to GSU because their real parameters during operation are unknown. Therefore, initializing the positions $\vec{\varphi}_i(0)$ and velocities $\vec{v}_i(0)$ of particles randomly in the whole problem hyperspace is necessary. In addition, iteration using the maximum cycle index $cyc_{\max}$ is necessary to find the optimal solution $\vec{\varphi}_{g\rm best}$ in the whole problem hyperspace. Doing so is time consuming but it can find the first optimal solution, which is the basis of *General Calculation Mode*.

2) General Calculation Mode: During operation, the inverter parameters (e.g., dc-link voltage and power factor) will change slowly in a limited range. The calculation process could spend less cycle index instead of the maximum cycle index to find the new optimal solution if position $\vec{\varphi}_i(0)$ is initialized to be the last optimal solution. In order to find the new optimal solution, velocities $\vec{v}_i(0)$ are still initialized randomly. Since the algorithm will only iterate the calculation limited times, the general calculation mode is highly efficient in implementation.

IV. Experimental Verifications

The constructed experimental prototype has four distributed single-phase inverters with their own independent dc sources, H-bridge circuits, output filters, and digital controllers as the picture shown in Fig. 16. All these inverter are connected to

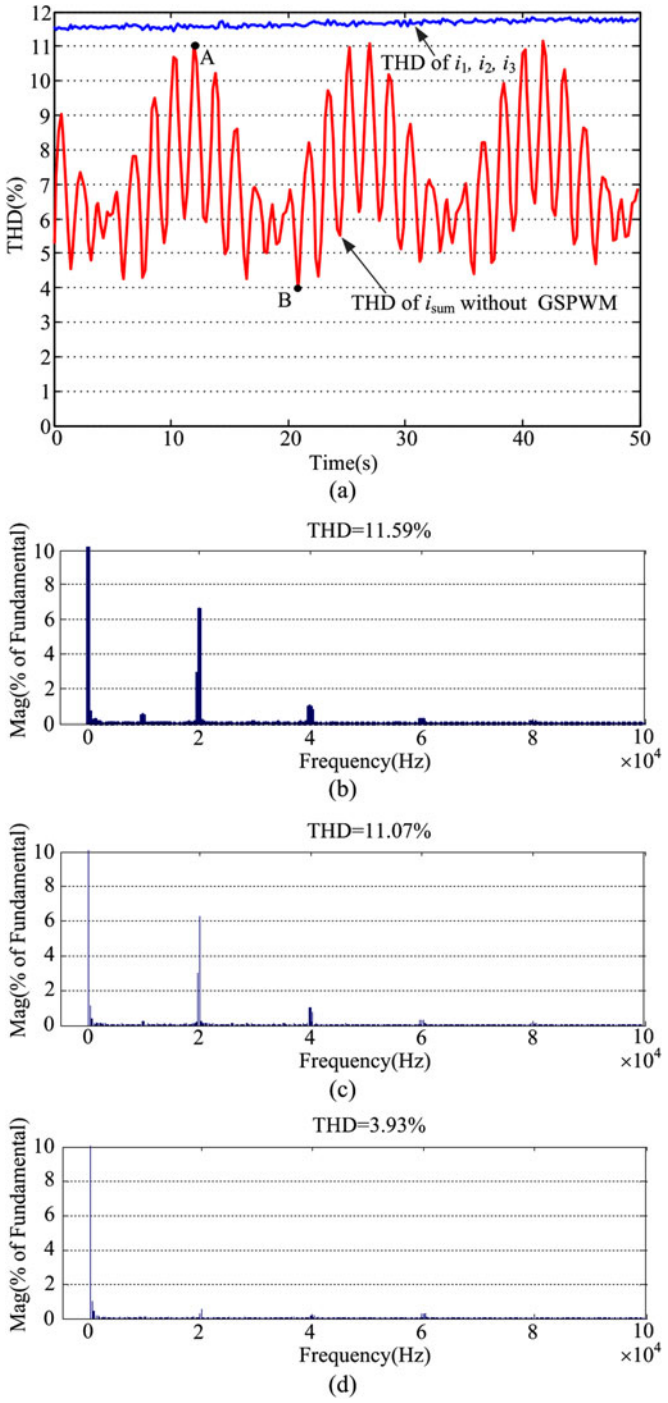

Fig. 17. Experimental results of three inverters without using GSPWM. (a) THD of i_1, i_2, i_3, $i_{\rm sum}$ in 50 s. (b) THD and FFT spectrum of i_1, i_2, i_3. (c) THD and FFT spectrum of $i_{\rm sum}$ at point A in (a). (d) THD and FFT spectrum of $i_{\rm sum}$ at point B in (a).

an emulated grid using a programmable ac source AMETEK-CI-4500LS, whose RMS value of output voltage is 110 V and output frequency is 50 Hz.

First, three inverters with the same operation parameters were used to verify the theory presented in Section II. In particular, $f_c = 10$ kHz, $f_1 = 50$ Hz, $U_{\rm dc} = 200$ V, and $L = 3.5$ mH. Fig. 17 presents the results without using GSPWM. In specific, Fig. 17(a) shows the THD of total current $i_{\rm sum}$ which changes as

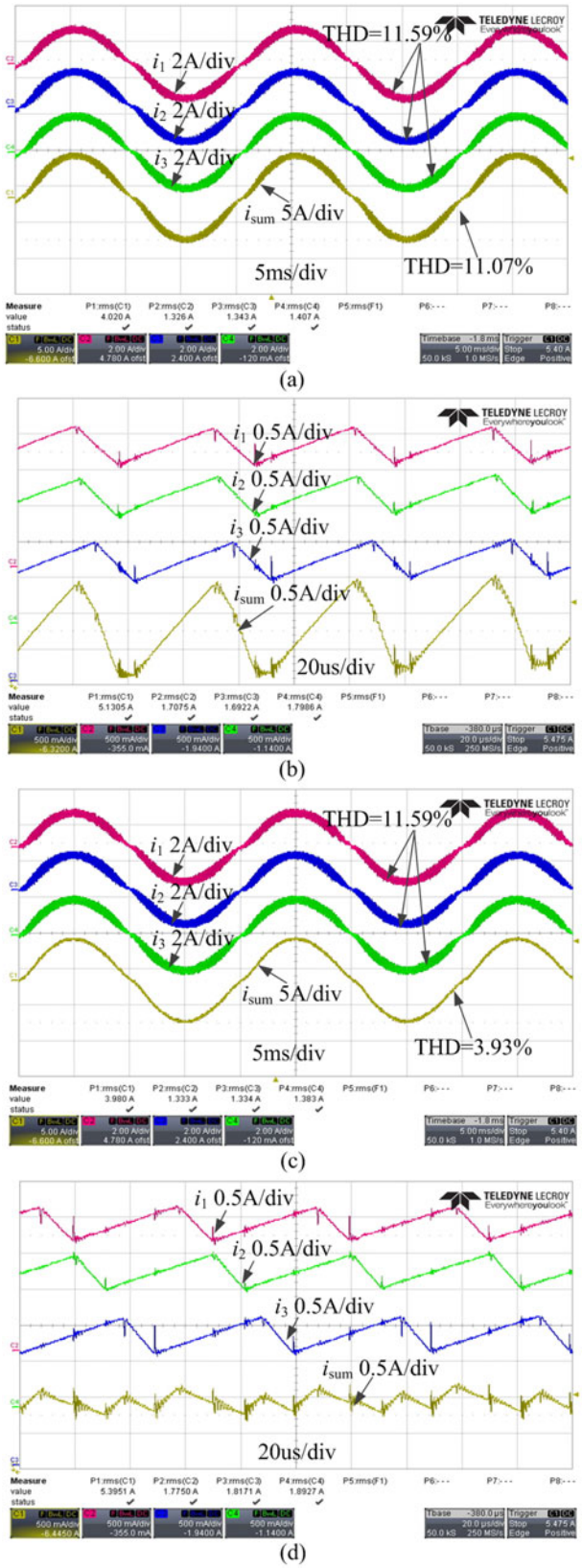

Fig. 18. Experimental waveforms of three inverters without using GSPWM. (a) Current waveform of i_1, i_2, i_3, $i_{\rm sum}$ at point A. (b) Zoomed view of (a). (c) Current waveform of i_1, i_2, i_3, $i_{\rm sum}$ at point B. (d) Zoomed view of (c).

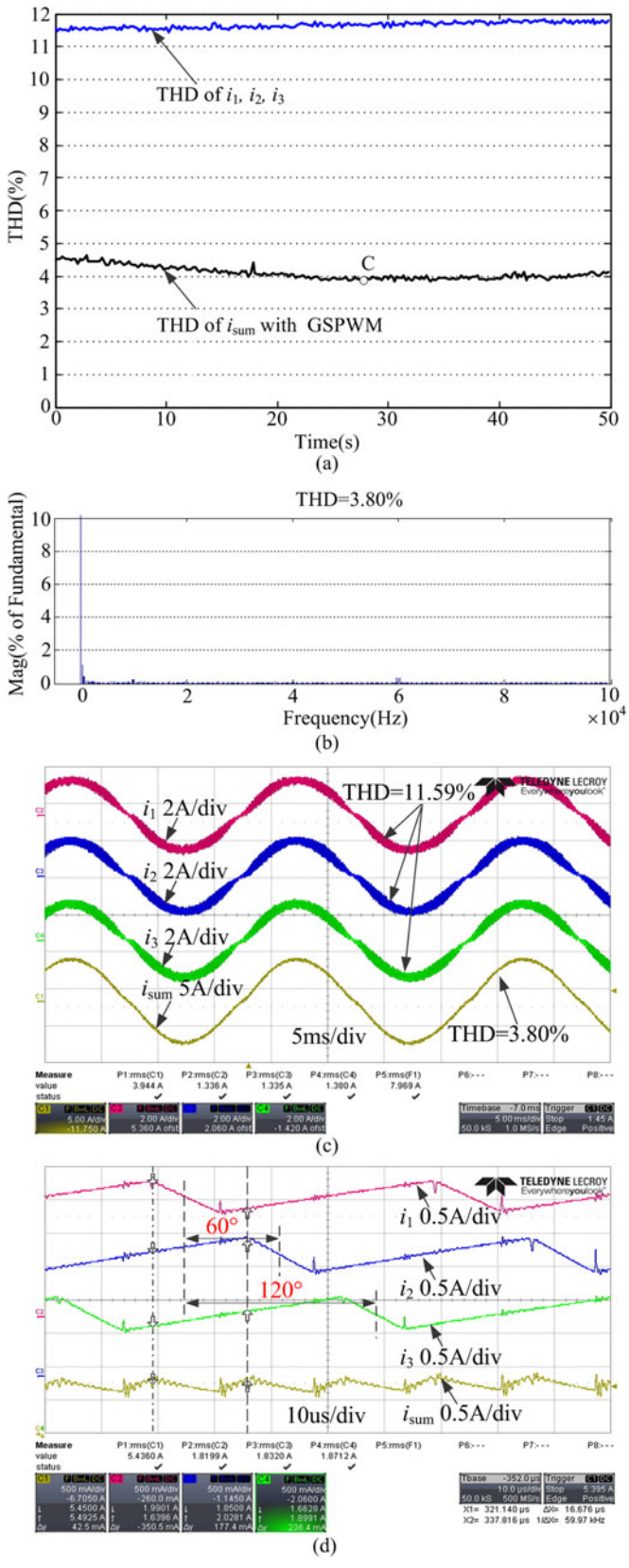

Fig. 19. Experimental results of three single-phase inverters when using GSPWM. (a) THD of i_1, i_2, i_3, $i_{\rm sum}$ in 50 s. (b) THD and FFT spectrum of $i_{\rm sum}$ at point C in (a). (c) Current waveforms of i_1, i_2, i_3, $i_{\rm sum}$ at point C in (a). (d) Zoomed view of (c).

TABLE III
PARAMETERS OF FOUR INVERTERS

M	$U_{\rm dcM}$ /V	$L_{\rm M}$ /mH	$f_{\rm cM}$ /kHz	$P_{\rm M}$ /W	Optimal phase-shift angles
1	210	3.4	10	156	0°
2	210	4.4	20	124	280°
3	190	4.4	10	218	34°
4	190	3.4	10	280	124°

time progresses and the THD of i_1, i_2, i_3. It could be seen that the THD of $i_{\rm sum}$ shown in Fig. 17(a) changes significantly as time progresses because the high-frequency current harmonics would be randomly summed. However, the THD of each inverter will not change much as demonstrated by its fast Fourier transform (FFT) spectrum shown in Fig. 17(b). Fig. 17(c) and (d) shows the THD and FFT spectrum of $i_{\rm sum}$ at point A and point B in Fig. 17(a), respectively. It is obvious that the THDs of $i_{\rm sum}$ at point A and B are much different, which further proves that the output currents are randomly accumulated at PCC. Fig. 18(a) and (b) shows the experimental current waveforms and zoomed view at point A in Fig. 17(a), respectively, where the current ripple of $i_{\rm sum}$ is large. Fig. 18(c) and (d) shows the experimental current waveforms and zoomed view at point B in Fig. 17(a), respectively. Comparatively, the current ripple of $i_{\rm sum}$ at point B is small.

Fig. 19 shows the experimental results when using GSPWM for three single-phase inverters. The calculation result of $f_{\rm synmin}$ is 10 Hz when setting the THD of total current should be lower than 5%, and $f_{\rm syn}$ is chosen as 50 Hz. Fig. 19(a) shows the THD of total current $i_{\rm sum}$ and the THD of i_1, i_2, i_3. Obviously, the THD of total current $i_{\rm sum}$ is small and almost constant because GSPWM can fix $\varphi_{\rm PWM2}$ and $\varphi_{\rm PWM3}$ at their optimal value $\varphi_{\rm PWM2best} = 60°$ and $\varphi_{\rm PWM3best} = 120°$ effectively. Fig. 19(b) shows the THD and FFT spectrum of $i_{\rm sum}$ at point C in Fig. 19(a). It can be seen that most of high-frequency harmonics have been attenuated. Fig. 19(c) and (d) shows the experimental current waveforms and zoomed view at point C, where the current ripple of $i_{\rm sum}$ is very small.

Next, to prove the proposed general method under complex working conditions, four single-phase inverters with different operational parameters are connected to the PCC. Table III shows the parameters of these four inverters. Fig. 20 presents the results without using GSPWM. Fig. 20(a) shows the THD of i_1, i_2, i_3, i_4, $i_{\rm sum}$ in 20 s. Being similar, the THD of $i_{\rm sum}$ varies significantly. Fig. 20(b) shows the THD and FFT spectrum of $i_{\rm sum}$ at point D in Fig. 20(a). Fig. 20(c) shows the THD and FFT spectrum of $i_{\rm sum}$ at point E in Fig. 20(a). Both results comply with the THD trajectory of Fig. 20(a). Fig. 21(a) shows the current waveforms of i_1, i_2, i_3, i_4, $i_{\rm sum}$ at point D and Fig. 21(b) shows the zoomed view of Fig. 21(a), where the current ripple of $i_{\rm sum}$ is large and uncertain since four inverters work under different conditions. Fig. 21(c) shows the current waveforms of i_1, i_2, i_3, i_4, $i_{\rm sum}$ at point E and Fig. 21(d) shows the zoomed view of Fig. 21(c). As expected, the current ripple is small.

When assuming GSPWM for these four inverters, $cyc_{\max}$ in *First Calculation Mode* and *General Calculation Mode* are set

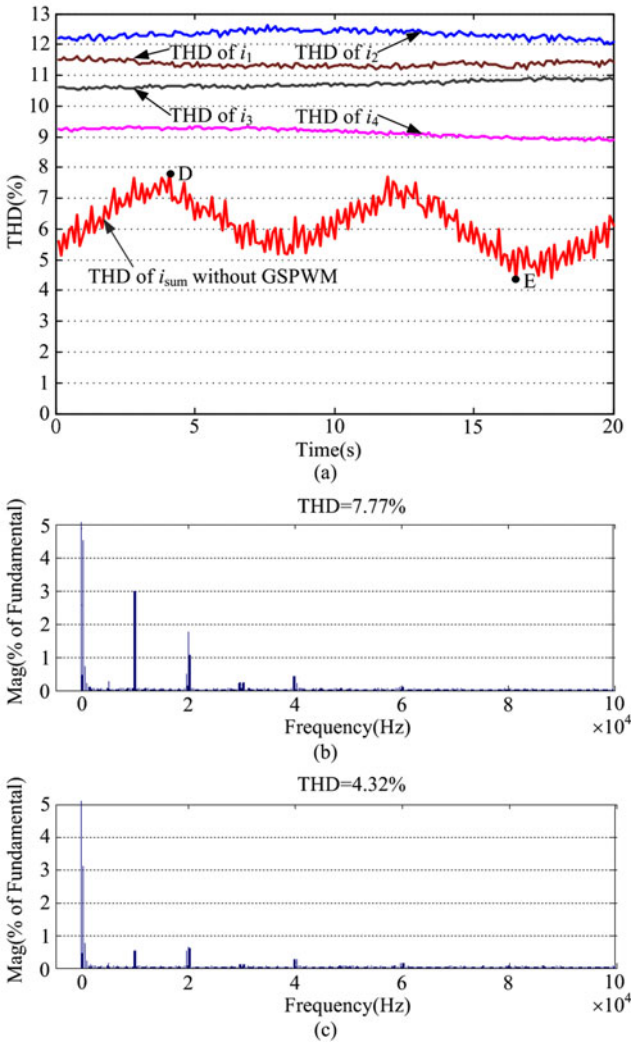

Fig. 20. Experimental results of four different single-phase inverters without using GSPWM. (a) THD of i_1, i_2, i_3, i_4, $i_{\rm sum}$ in 20 s. (b) THD and FFT spectrum of $i_{\rm sum}$ at point D in (a). (c) THD and FFT spectrum of $i_{\rm sum}$ at point E in (a).

to be 100 and 20, respectively, $X_{\max}$ is set as 20 to get the qualified results. It cost DSP(TMS320F28335) 2 s to calculate the optimal phase-shift angles and $f_{\rm syn}$ under the *First Calcuation Mode*. The calculation result of $f_{\rm synmin}$ is 24 Hz when setting the THD of $i_{\rm sum}$ should be lower than 5%, and $f_{\rm syn}$ is chosen as 50 Hz either. The calculated phase angles for these four inverters are $\varphi_{\rm PWM1best} = 0°$, $\varphi_{\rm PWM2best} = 280°$, $\varphi_{\rm PWM3best} = 34°$, and $\varphi_{\rm PWM4best} = 124°$, respectively. Comparatively, Fig. 22 shows the experimental results of these four single-phase inverters when using the proposed GSPWM method. The green line in Fig. 22(a) represents the THD trajectory of $i_{\rm sum}$ in 20 s, which could keep almost unchanged during operation and is much lower than the output current THD of individual inverter. Fig. 22(b) shows the THD and FFT spectrum of $i_{\rm sum}$ at point F in Fig. 22(a). Fig. 22(c) and Fig. 22(d) show the experimental current waveforms and zoomed view at point F in Fig. 22(a), where the current ripple of $i_{\rm sum}$ is attenuated by properly maintaining the optimal phase-shift angles between four inverters.

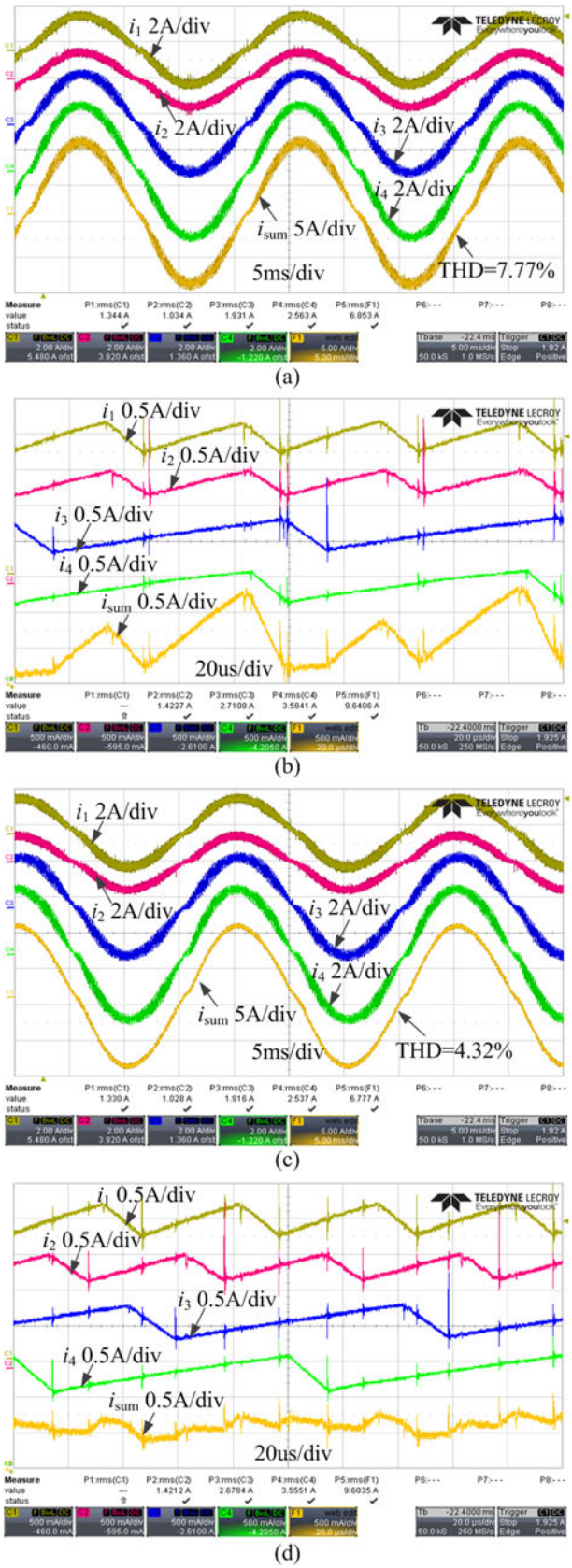

Fig. 21. Experimental waveforms of four different single-phase inverters without using GSPWM. (a) Current waveforms of i_1, i_2, i_3, i_4, $i_{\rm sum}$ at point D. (b) Zoomed view of (a). (c) Current waveforms of i_1, i_2, i_3, i_4, $i_{\rm sum}$ at point E. (d) Zoomed view of (c).

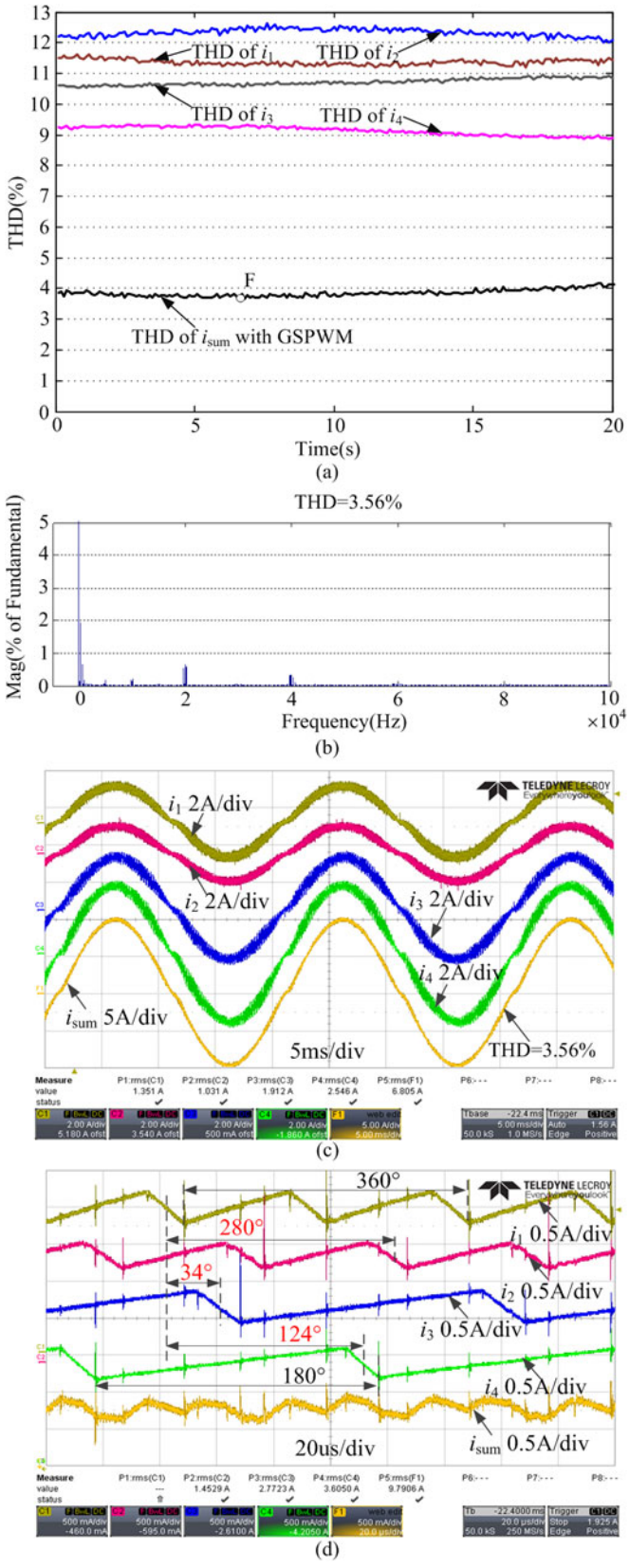

Fig. 22. Experimental results of four different single-phase inverters when using GSPWM. (a) THD of i_1, i_2, i_3, i_4, $i_{\rm sum}$ in 20 s. (b) THD and FFT spectrum of $i_{\rm sum}$ at point F in (a). (c) Current waveforms of i_1, i_2, i_3, i_4, $i_{\rm sum}$ at point F in (a). (d) Zoomed view of (c).

V. Conclusion

This paper proposes a GSPWM method for multiple distributed inverters to attenuate the high-frequency current harmonics at PCC. With highly reliable communication system, the proposed method can lead to the reduction of filter size or switching frequency per inverter. The global synchronization is realized through the communication channel of RS485 and the GSU in this paper. The optimal interleaved switching angles among distributed inverters are calculated by fully considering line impedances, modulation indexes, switching frequencies, the number of distributed inverters, etc. PSO method is used to find the optimal phase-shift angels and synchronization frequency among multiple distributed inverters. Experimental results verified the performance of the proposed GSPWM.

References

[1] F. Blaabjerg, Z. Chen, and S. B. Kjaer, "Power electronics as efficient interface in dispersed power generation systems," *IEEE Trans. Power Electron.*, vol. 19, no. 5, pp. 1184–1194, Sep. 2004.

[2] F. Blaabjerg, R. Teodorescu, M. Liserre, and A. V. Timbus, "Overview of control and grid synchronization for distributed power generation systems," *IEEE Trans. Ind. Electron.*, vol. 53, no. 5, pp. 1398–1409, Oct. 2006.

[3] Y. Xue, L. Chang, S. B. Kjær, J. Bordonau, and T. Shimizu, "Topologies of single-phase inverters for small distributed power generators: An overview," *IEEE Trans. Power Electron.*, vol. 19, no. 5, pp. 1305–1314, Sep. 2004.

[4] I. J. Gabe, V. F. Montagner, and H. Pinheiro, "Design and implementation of a robust current controller for VSI connected to the grid through an LCL filter," *IEEE Trans. Power Electron.*, vol. 24, no. 6, pp. 1444–1452, Jun. 2009.

[5] H. Cha and T.-K. Vu, "Comparative analysis of low-pass output filter for single-phase grid-connected Photovoltaic inverter," in *Proc. 25th Annu. Appl. Power Electron. Conf. Expo.*, 2010, pp. 1659–1665.

[6] K. H. Ahmed, S. J. Finney, and B. W. Williams, "Passive filter design for three-phase inverter interfacing in distributed generation," in *Proc. Compat. Power Electron.*, 2007, pp. 1–9.

[7] A. Houari, H. Renaudineau, J. P. Pierfedrici, and F. Meibody-Tabar, "Flatness based control of three phase inverter with output LC filter," *IEEE Trans. Ind. Electron.*, vol. 59, no. 7, pp. 2890–2897, Jul. 2012.

[8] G. Ding, F. Gao, Y. Tang, L. Zhang, and S. Zhang, "A novel harmonic control approach of distributed generation converters in a weak microgrid," in *Proc. Annu. Appl. Power Electron. Conf. Expo.*, 2014, pp. 2132–2139.

[9] M. Liserre, F. Blaabjerg, and S. Hansen, "Design and control of an LCL filter-based three-phase active rectifier," *IEEE Trans. Ind. Appl.*, vol. 41, no. 5, pp. 1281–1291, Sep./Oct. 2005.

[10] E. Twining and D. Holmes, "Grid current regulation of a three-phase voltage source inverter with an LCL input filter," *IEEE Trans. Power Electron.*, vol. 18, no. 3, pp. 888–895, May 2003.

[11] M. Liserre, A. D. Aquilla, and F. Blaabjerg, "Genetic algorithm based design of the active damping for an LCL-filter three-phase active rectifier," *IEEE Trans. Power Electron.*, vol. 19, no. 1, pp. 76–86, Jan. 2004.

[12] M. A. Abusara and S. M. Sharkh, "Design and control of a grid-connected interleaved inverter," *IEEE Trans. Power Electron.*, vol. 28, no. 2, pp. 748–764, Feb. 2013.

[13] P. J. Grbovic, "Closed form analysis of N-cell interleaved two-level DC-DC converters: The DC bus capacitor current stress," in *Proc. ECCE Asia Downunder*, 2013, pp. 122–129.

[14] B. Cougo, T. Meynard, and G. Gateau, "Parallel three-phase inverters: Optimal PWM method for flux reduction in intercell transformers," *IEEE Trans. Power Electron.*, vol. 26, no. 8, pp. 2184–2191, Aug. 2011.

[15] D. M. Vilathgamuwa, C. J. Gajanayake, and P. C. Loh, "Modulation and control of three-phase paralleled Z-source inverters for distributed generation applications," *IEEE Trans. Energy Convers.*, vol. 24, no. 1, pp. 173–183, Mar. 2009.

[16] D. Perreault and J. Kassakian, "Distributed interleaving of paralleled power converters," *IEEE Trans. Circuits Syst. I, Fundam. Theory Appl.*, vol. 44, no. 8, pp. 728–734, Aug. 1997.

[17] T. Beechner and J. Sun, "Asymmetric interleaving—A new approach to operating parallel converters," in *Proc. Energy Convers. Congr. Expo.*, 2009, pp. 99–105.
[18] M. Schuck and R. C. N. Pilawa-Podgurski, "Ripple minimization in asymmetric multiphase interleaved DC-DC switching converters," in *Proc. Energy Convers. Congr. Expo.*, 2013, pp. 133–139.
[19] B. Singh, K. Al-Haddad, and A. Chandra, "A review of power quality improvement," *IEEE Trans. Ind. Electron.*, vol. 46, no. 5, pp. 960–971, Oct. 1999.
[20] X. Yuan, W. Merk, H. Stemmler, and J. Allmeling, "Stationary-frame generalized integrators for current control of active power filters with zero steady-state error for current harmonics of concern under unbalanced and distorted operating conditions," *IEEE Trans. Ind. Appl.*, vol. 38, no. 2, pp. 523–532, Mar./Apr. 2002.
[21] R. W. Rhea, *Discrete Oscillator Design: Linear, Nonlinear, Transient, and Noise Domains*. Norwood, MA, USA: Artech House, 2014, pp. 332–334.
[22] S. Jayawant and J. Sun, "Double-integral Fourier analysis of interleaved pulse width modulation," in *Proc. Comput. Power Electron. Workshop*, 2006, pp. 34–39.
[23] D. Holmes and T. Lipo, *Pulse Width Modulation for Power Converters: Principles and Practice*. New York, NY, USA: Wiley, 2003.
[24] J. Kennedy and R. C. Eberhart, "Particle swarm optimization," in *Proc. IEEE Int. Conf. Neural Netw.*, 1995, pp. 1942–1948.
[25] R. Eberhart and J. Kennedy, "A new optimizer using particle swarm theory," in *Proc. 6th Int. Symp. Micro Mach. Human Sci.*, 1995, pp. 39–43.
[26] Y. Del Valley, G. K. Venayagamoorthy, S. Mohagheghi, J.-C. Hernandez, and R. G. Harley, "Particle swarm optimization: Basic concepts, variants and applications in power systems," *IEEE Trans. Power Del.*, vol. 12, no. 2, pp. 171–195, Apr. 2008.
[27] J. Kennedy, "The particle swarm: Social adaptation of knowledge," in *Proc. IEEE Int. Conf. Evol. Comput.*, 1997, pp. 303–308.
[28] E. Ozcan and C. Mohan, "Particle swarm optimization: Surfing the waves," in *Proc. IEEE Congr. Evol. Comput.*, 1999, vol. 3, pp. 1939–1944.

Tao Xu received the B.Eng. degree in electrical engineering from Shandong University, Jinan, China, in 2014, where he is currently working toward the Ph.D. degree.

His research interests include power quality, ac/dc microgrid, and modulation methods.

Feng Gao (S'07–M'09) received the B.Eng. and M.Eng. degrees in electrical engineering from Shandong University, Jinan, China, in 2002 and 2005, respectively, and the Ph.D. degree from the School of Electrical and Electronic Engineering, Nanyang Technological University, Singapore, in 2009.

From 2008 to 2009, he was a Research Fellow in Nanyang Technological University. Since 2010, he joined the School of Electrical Engineering, Shandong University, where he is currently a Professor and serving as a Vice Dean. From September 2006 to February 2007, he was a Visiting Scholar at the Institute of Energy Technology, Aalborg University, Aalborg, Denmark.

Dr. Gao received the IEEE Industry Applications Society Industrial Power Converter Committee Prize for a paper published in 2006, and he is currently an Associate Editor of the IEEE TRANSACTIONS ON POWER ELECTRONICS.